Investigating the doping effects of Pb concentration on the optical & electrical properties of CdS Colloidal Quantum Dots

By

Henock Tadele Demissie

A THESIS SUBMITTED TO

GRADUATE PROGRAM OF

ADDIS ABABA UNIVERSITY

INPARTIAL FULFILLMENT OF THE REQUIREMENTS

FOR THE DEGREE OF

MASTERS OF SCIENCE IN PHYSICS

(POLYMER PHYSICS)

ADDIS ABABA, ETHIOPIA

AUGUST 2024

ADDIS ABABA UNIVERSITY

PROGRAM OF GRADUATE STUDIES

Investigating the doping effects of Pb concentration on the optical & electrical properties of CdS Colloidal Quantum Dots

By

Henock Tadele Demissie

Department of Physics

Addis Ababa University

Approved by the Examining Board

Chairperson: ----------

Signature

External Examiner: ----------

Signature

Internal Examiner: ----------

Signature

Advisor: ----------

Signature

Date: August 2024

ADDIS ABABA UNIVERSITY

Date: August 2024

Author: Henock Tadele Demissie

Title: Investigating the doping effects of Pb concentration on the optical & electrical properties of CdS Colloidal Quantum Dots

Department: Department of Physics

Degree: M.Sc. **Convocation:** August **Year:** 2024

Permission is here with granted to Addis Ababa university to circulate and to have copied for non-commercial, purposes, at its discretion, the above title upon the request of individuals or institution.

Signature of Author

This Work is Dedicated to My Family.

Acknowledgment

I would like to take this opportunity to express my deepest gratitude and appreciation to all those who have supported and guided me throughout the completion of this thesis.
First and foremost, I thank the Almighty God, His Holy Mother The Virgin Saint Mary and All the Heavenly Host for keeping me and guiding me through every second of my life. *"My Soul Finds Rest in God Alone; My Salvation comes from Him. He is my Rock and Salvation; He is my Fortress, I Will Never be Shaken." Psalms 61:1-2*
I owe a special debt of gratitude to my family for their unwavering support, love, and understanding throughout this entire process. Their belief in me and their encouragement during moments of doubt have been the driving force behind my perseverance and determination.
I am immensely grateful to my thesis supervisor, *Prof.* Fekadu Gashaw, for their unwavering guidance, expertise, encouragement and providing the lab infrastructure. Their invaluable insights, constructive feedback, and dedication have been instrumental in shaping the direction and quality of this research. I am truly fortunate to have had their mentorship throughout this journey.
I extend my heartfelt thanks to *Dr.* Newayemedhin Aberra for their thoughtful suggestions, experimental lab analysis, and scholarly input which have significantly strengthened this thesis and enriched its content.
I would also like to acknowledge the contributions of my colleagues and friends from the material science group who have provided support and encouragement during this challenging endeavor. I can not thank Mr. Simenew enough for his continued support in time, resource and guidance in the lab. Mr. Lema for his feedback on the concepts, experimental work and characterization results. Dr. Nika, Mr. Kassa, Mrs. Kidan, Mr. Eninges, Mr. Gizaw for their willingness to share their insights, knowledge, experiences and guidance have been immensely helpful in refining my ideas and expanding my perspective. Additionally, I would like to thank Mrs. Helen for her immense help in organizing this paper.
Lastly, I would like to express my appreciation to the Chemistry Department for providing the photoluminescence and FTIR characterizations.

Abstract

In the present study, the doping effect of lead (Pb) atoms on the optoelectronic properties of cadmium sulfide (CdS) colloidal quantum dots is investigated. The concept of quantum confinement has been explored, emphasizing the role of Quantum Mechanics and the effective mass approximation in understanding confinement energy. Experimental synthesis of CdS colloidal quantum dots was performed using a modified method of chemical bath deposition technique. The resulting quantum dots exhibited a bright yellow vibrant color. UV-Vis and PL studies revealed a redshift followed by a blueshift at increased Pb concentrations. Tauc plot analysis determined the bandgap values to be 2.70eV, 2.67eV, 2.72eV, 2.74eV and 2.77eV for pure, 0.10%, 0.15%, 0.20% and 0.25% doped samples respectively. This increase in bandgap was attributed to the Burstein-Moss effect. FTIR characterization showed shifts and intensity changes in peaks of the fingerprint region, indicating variations in molecular vibrations and stretching due to Pb doping. Optical analysis provided insights into the refractive index, dielectric constant, and linear optical susceptibility, which decreased with increasing bandgap. The electrical characterization showed decrease in resistivity and augmented conductivity by upto 7 times from the undoped sample with higher Pb concentrations. Moreover, the IV curve exhibited an ohmic nature, suggesting the samples resemble metallic conductor properties.

Keywords: Quantum Dots, Doping, Bandgap, Quantum Confinement Effect, Burstein-Moss Effect

Contents

List of Tables

List of Figures

Acronyms

BM Shift Burstein-Moss Shift

CB Conduction Band

CBD Chemical Bath Deposition

CdS Cadmium Sulfide

CQDs Colloidal Quantum Dots

EDX Energy Dispersive X-ray Spectroscopy

EXAFS Extended X-ray Absorption Fine Structure

FTIR Fourier Transform Infrared Spectroscopy

FWHM Full Width at Half Maximum

HRTEM High Resolution Transmission Electron Microscopy

Pb Lead

PL Photoluminescence Spectroscopy

QDSSC Quantum Dot Sensitized Solar Cell

SILAR Successive Ionic Layer Adsorption And Reaction

TEM Transmission Electron Microscopy

UV Ultraviolet

VB Valence Band

XANES X-ray Absorption Near Edge Spectroscopy

XPS X-ray Photoelectron Spectroscopy

XRD X-Ray Diffraction Analysis

Chapter 1

Introduction

Semiconductors, the backbone of modern technology, have revolutionized the way we live, work, and communicate. In the past century semiconductor devices have brought about an abrupt advancement and growth in technology, providing human beings to design, integrate, harvest energy and communicate easily. These remarkable materials, with their unique electrical properties, form the foundation of electronic devices that power our digital age. From smartphones and computers to solar cells and sensors, semiconductors have transformed our world[1].

Nanotechnology is a leading interdisciplinary science that is emerging as a distinctive field of research. Its advances and applications will result in technical capabilities that will allow the development of novel nanomaterials with applications that will revolutionize the industry in many areas[2]. Quantum dots, nanoscale semiconductor particles with extraordinary optical and electronic properties, have emerged as a promising area of research with immense potential for various applications. By harnessing the principles of Quantum Mechanics, these tiny structures exhibit size-dependent behavior, enabling precise control over their optical and electronic properties.

In this thesis introduction, we will explore the fascinating world of quantum dots, their unique characteristics, the quantum confinement effect and the implications in lead doped cadmium sulfide quantum dots.

1.1 Working on Nanoscale: From Bulk to QDs

The properties of bulk materials, defined as those materials with all dimensions greater than 100 nm in length, are constant, independent of their dimensions. However, as we move into the nanoscale region, defined by at least one dimension of the material being in the region of 1-100nm, the physical and electronic properties of the material vary depending on their size. This is a consequence of both the greatly increased surface area to volume ratio of nanomaterials and the quantum confinement of the electrons, which will be explained later, leading to properties bridging bulk and molecular characteristics. The area of nanoscience has received great interest since Richard Feynman gave his seminal speech, *'There's plenty of room at the bottom'* in 1959, outlining the great potential of working on the nanoscale[3]. More

recent advancements in microscopy techniques, in particular electron microscopes, have advanced the field greatly with the ability to image materials on the nanoscale allowing close study of atoms and molecules on the nanolevel as shown in figure 1.1. These developments have led to nanoscience being incorporated into many different applications today and is expected to continue to be the basis for many technological advancements over the coming decades.

The comparison between bulk systems and nanomaterials obviously arises from dimension

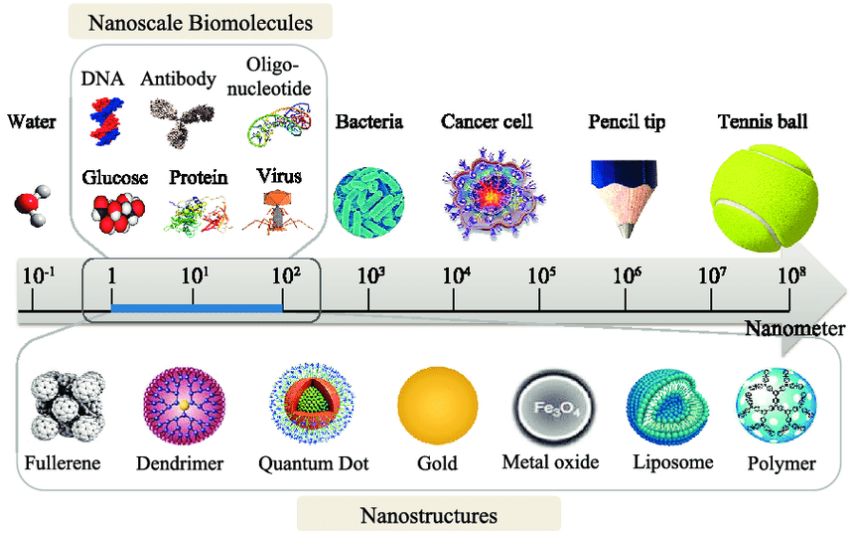

Figure 1.1: The Nanoscale Diagram *Source: Saallah, S; Lenggoro, W, 2018*

differences, however, such difference in scaling also gives rise to other properties which are crucial for distinction between the two systems. These properties are summarised in Table 1.1.

Table 1.1: Comparison between Bulk and Nanomaterials

Property	**Bulk Material**	**Nanomaterials**
Size	Macroscopic dimensions, typically in μm or mm	Microscopic dimensions, typically ranging from 1 to 100nm
Structure	3 Degrees of Freedom (DF) and Zero Degree of Confinement (DC)	Depending on the type of nanomaterial, can have 2 DF (1-DC), 1 DF (2-DC), 0 DF (3-DC)
Electronic	Continuous Energy Bands	Discrete and Quantized Energy Levels
Optical	Continuous absorption and emission spectrum	Size dependent absorption and emission properties
Quantum Effects	No quantum effect	Quantum mechanics governs the properties of the nanomaterial

1.2 Quantum Dots *"The Seeds of Nanoscience"*

An element's properties are determined by its electronic configuration, but Quantum phenomena emerge when matter is reduced to nanoscale dimensions due to matter size[4], [5]. QDs were first discovered by Aleksey Yekimov in a glass matrix in 1980 and by R. Rossetti & Louis Brus in colloidal solution in 1985. As such the Chemistry Nobel Prize for 2023 recognizes the discovery and evolution of quantum dots (QDs) and is jointly awarded to Aleksey Yekimov (created size-dependent quantum effects in coloured glass), Louis Brus (first to demonstrate size-dependent particle quantum effects), and Moungi Bawendi (revolutionized the chemical productions of QD)[6]. QDs are tiny nanoparticles with properties determined by size. They constitute a new class of materials that are neither molecular nor bulk. The Royal Swedish Academy of Sciences describes these intriguing semiconductors as materials having the same structure and atomic composition as bulk materials, but their properties can be tuned using a single parameter, the particle's size.

Quantum dots are considered as particles with zero dimensions lying mostly in between 1-10 nm scale. Particles with zero dimension can be considered as 3D confined particle i.e. particle bound to a system and thus have discrete energy levels. If a particle is 1D confined the particle is termed as Quantum well, if the particle is 2D confined particle it is termed as Quantum wire and if 3D confinement is there, the particle is termed as Quantum Dot. Their electronic and optical properties vary from bulk particles[7]. Electronic properties lie between bulk semiconductors and discrete molecules, and optical properties like band gap can be tuned according to its size. Band gap of semiconducting material increases with decrease in its size. As size of QDs decreases, color shift occurs from red to blue, resulting QDs of same material exhibit different types of color as according to its size[8]. In 1996, Alivisatos showed that basic physical phenomenon of quantum confinement arises because of change in electronic states[9]. We can understand this confinement by considering the relation between position and momentum in confined and free particles. Due to their small size and discrete energy levels, they exhibit different optical and electronic properties from bulk counterparts. For example, in UV-Vis absorption spectroscopy QDs show blue shift compared to bulk particles[10]. Also while calculating the bandgap from UV-Vis absorption data, increase in bandgap was observed showing that their bandgap can be tuned by varying their size. The advent of reliable production of nano-structures has opened a frontier in material science. As the size of these structures or devices approaches the nanometer scale the laws of quantum mechanics come into play. Quantum dot structures are being considered for a variety of technological applications ranging from semiconductor electronics to biological

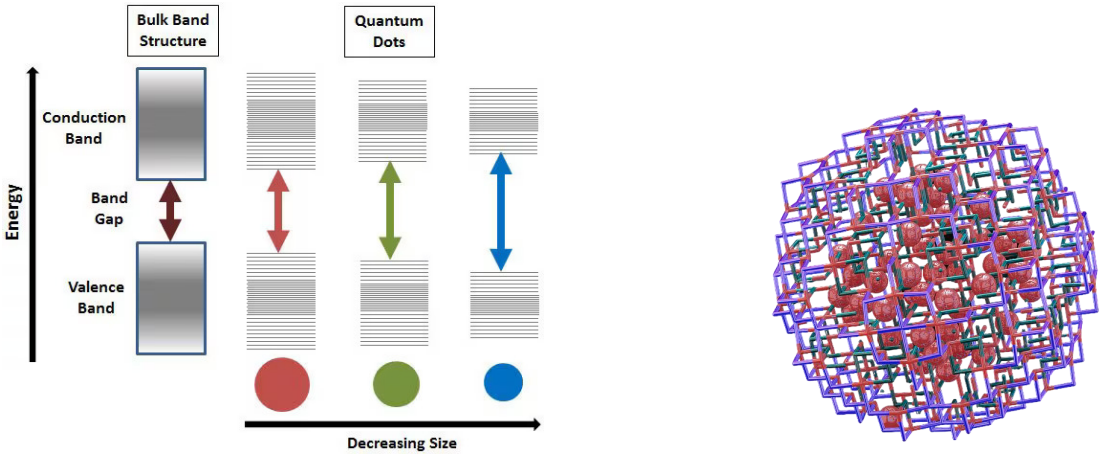

Figure 1.2: **(a)**Size-Dependent band gap Variation in QDs **(b)**Simulation Model of Spherical QD *Source: P. Subhapriya, 2023*

applications including optical devices, quantum communications and quantum computing as listed in section 1.5. The understanding of the quantum structure's electronic properties and quantum confinement is of paramount importance. The basic concept of quantum confinement comes from the interplay of two fundamental principles of quantum mechanics; namely the electronic system must obey the Schrödinger equation and also follow the De Broglie momentum-wavelength relationship. As such a quantum dot is a semiconductor nano-structure that confines the motion of conduction band electrons, valence band holes, or excitons (quasiparticle bound pairs of electrons and holes) in all three spatial directions [11].

1.3 Quantum Mechanical Treatment of Quantum Dots

A fundamental aspect of quantum mechanics is the particle-wave duality, as introduced by De Broglie, according to which any particle can be associated with a matter wave, the wavelength λ of which is inversely proportional to the particle's linear momentum p[1].

$$\lambda = \frac{h}{p} = \frac{h}{mv} \tag{1.1}$$

where h is the Plank's Constant

Whenever the size of a physical system becomes comparable to the wavelength of the particles, the behaviour of the particle is best described by the rules of quantum mechanics. The electronic structure of bulk semiconductor crystals is described correctly by the band theory

where the electron states are not distributed in discrete levels as in atoms and molecules, rather form continuous bands, namely conduction and valence bands, which are separated by an energy gap E_g[12]. In nanostructured semiconductors, the band structure model is no longer sufficient to explain the electronic structure and other alternative models must be considered. As a result, due to consequences of nano-dimenison quantum mechanical concepts such as quantum confinement, quantization of energy, discrete energy levels and uncertainity principle are used to describe the electronic structures and properties in such semiconductors. An important phenomena called Quantum confinement occurs when the De Broglie wavelengths of electrons λ_e and holes λ_h and the Bohr radius a_B are in the order or greater than the spatial dimensions of the crystal. This situation can hold for one, two or three directions in space. Therefore, one can have 1-, 2- and 3- dimensional quantum confinement[13].

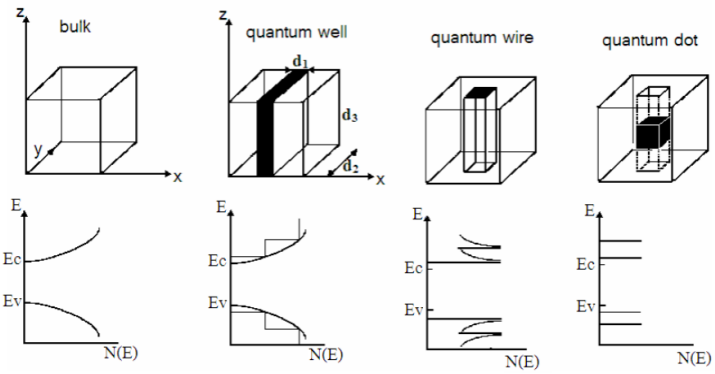

Figure 1.3: Density of States of semiconducting material for bulk, 2D, 1D and 0D crystals.[14]

1.3.1 Density of States

The effects of low dimensionality are immediately visible in the density of states (DOS) of a semiconductor nanoparticle. At the diminishing of the size, the continuous bands become discrete i.e. they assume an atom-like aspect. QDs are composed of approximately $10^2 - 10^4$ atoms, as a result they exhibit distinct narrow optical line spectra. This is why, QDs are often described as artificial atoms. When considering the DOS for 0D structure, no free motion is possible. Since there is no k-space to be filled with electrons and all available states exist only at discrete energies, the DOS is then described by the delta function as shown in figure 1.3[9].

$$D(E) = 2\delta(E - E_F) \tag{1.2}$$

1.3.2 Nature of Carriers in QDs

Carriers in any condensed matter system define optoelectronic properties of such system. Quantum dots provide confinement for carriers in all three spatial dimensions giving rise to the atomic-like discrete spectrum. This can be very useful in optoelectronic applications since semiconductor technology is already very well developed while discreteness of the spectrum may provide very interesting features for possible optoelectronic applications. All optoelectronic applications are physically based on interaction of external electromagnetic field and charge carriers inside the considered system. The term "carrier" in quantum dots may refer to electrons, holes, excitons and even polarons as a carriers of charge. Undoped QDs has all the electrons in valence band in thermodynamical equilibrium. Only few electrons from valence band can be thermally or optically excited providing electrons in conduction band and leaving holes in valence band. Electrons and holes act as carriers, but they also interact mutually by Coulomb forces forming excitons[15]. However, the binding energy required to create one is much smaller than the thermal energy; therefore, excitons have a very low probability of existing in a bulk semiconductor at room temperature. In quantum confined systems, and particularly in QDs, the excited electron and hole are forced to exist very close to each other, causing large Coulomb interactions between them. In this case, the binding energy and oscillator strengths are increased, hence the excitons can exist at room temperature[16].

1.3.3 Quantum Confinement Effect

Quantum confinement is the spatial confinement of electron–hole pairs (excitons) in one or more dimensions within a material. For a free particle with effective mass m* confined in a crystal by impenetrable barriers (i. e., infinite potential energy) in the z direction, the allowed wavevectors k_z of the Bloch waves are given by[12]:

$$k_{zn} = \frac{2\pi}{\lambda_n} = \frac{n\pi}{L} \tag{1.3}$$

where n=1,2,3...
The ground state energy is increased by the amount ΔE relative to the unconfined case:

$$\Delta E = \frac{\hbar^2 k_{z1}^2}{2m^*} = (\frac{\hbar^2}{2m^*})(\frac{\pi^2}{L^2}) \tag{1.4}$$

This increase in energy is referred to as the confinement energy of the particle. It is a consequence of the uncertainty principle in quantum mechanics. When the particle is confined

within a distance L in space (along the z direction in this case) the uncertainty in the z component of its momentum increases by an amount of the order of $\hbar/L$. The corresponding increase in the particle's kinetic energy is then given by (1.4). Hence, this effect is known also as quantum confinement. In addition to increasing the minimum energy of the particle, confinement also causes its excited state energies to become quantized. Depending on the ratio of particle size D to the Bohr radius a_B of the exciton, the degree of confinement can be classified into three main categories[13]:

1. Strong Confinement: The size of the quantum dot is less than the Bohr radius for both the electron and hole ($D << a_B$)

2. Intermediate Confinement: The size of the quantum dot is less than the Bohr radius of one of the electron or hole, but not the other ($a_{Bh} < D < a_{Be}$)

3. Weak Confinement: The size of the quantum dot is greater than the Bohr radius of both the electron and hole ($D >> a_B$)

1.3.4 Effective Mass Approximation Model

This approach, based on the 'Particle-in-Box Model', is the most widely used model to predict quantum confinement. It was first proposed by Efros and Efros in 1982 and later modified by Brus. In this approximation model, an exciton is considered to be confined to a spherical volume of the crystallite and the mass of electron and hole is replaced with effective masses (m_e and m_h) to define the Hamiltonian $\hat{H}$ and the wave function[17].

1.3.4.1 Determination of Confinement Energy

An ideal spherical quantum dot is a spherical shaped semiconductor nanocrystal in which excitons are confined in an infinite spherical well[18]. This corresponds to an impenetrable hard spherical wall. The confining potential is given by[19]:

$$V(r) = \begin{cases} 0, & r \leq a \\ \infty, & otherwise \end{cases}$$

Where, r = radius of the confining potential and a = radius of the quantum dot

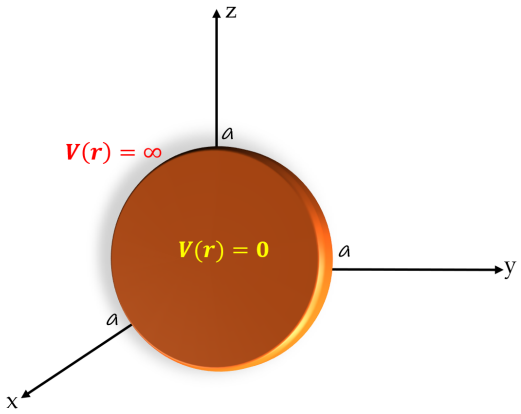

Figure 1.4: Infinite Spherical Potential Well with radius a

Following Schrödinger's time-independent wave equation (Davies, 2005):

$$\hat{H}\psi(\mathbf{r}) = E\psi(\mathbf{r}) \tag{1.5}$$

With the Hamiltonian operator $\hat{H}$ given as[20]:

$$\hat{H} = -\frac{\hbar^2}{2m_e^*}\nabla_e^2 - \frac{\hbar^2}{2m_h^*}\nabla_h^2 - \frac{e^2}{\epsilon_o|r_e - r_h|} \tag{1.6}$$

where the subscripts e and h represent electron and hole respectively. However, for ease of calculation we can represent the effective masses of electron m_e^* and hole m_h^* with the reduced mass μ, giving the general form of the Hamiltonian of the QD in the Schrödinger equation:

$$-\frac{\hbar^2}{2\mu}\nabla^2\psi(\mathbf{r}) + V(\mathbf{r})\psi(\mathbf{r}) = E\psi(\mathbf{r}) \tag{1.7}$$

Since the potential depends on the radius from a fixed point of a spherical quantum dot, the Laplacian ∇^2 of the spherical polar coordinate is independent of the angular part and is given as:

$$\nabla^2 = \frac{1}{r^2}\frac{\partial}{\partial r}\left(r^2\frac{\partial}{\partial r}\right) \tag{1.8}$$

Putting (1.8) into (1.7) for V(**r**)=0 in the region r≤ a we have:

$$-\frac{\hbar^2}{2\mu}\frac{1}{r^2}\frac{\partial}{\partial r}\left(r^2\frac{\partial}{\partial r}\right)\psi(\mathbf{r}) = E\psi(\mathbf{r}) \tag{1.9}$$

If we assume that the QD is spherical, decoupling of the Schrodinger equation into a radial part (depending on r) and a spherical harmonic part (depending on the angles θ and ϕ) is

possible. This decouplinng method is often quite good since most chemically synthesized nanocrystals have aspect ratios (defined as the ratio between the longest and shortest axes) smaller than 1. Hence, based on this assumption, $\psi(\mathbf{r}) = R(r)G(\theta)Q(\phi)$; the radial part of (1.9) by means of separation of variable yields:

$$\frac{1}{R}\frac{d}{dr}\left(r^2\frac{dR}{dr}\right) + \frac{2\mu E r^2}{\hbar^2} = l(l+1) \tag{1.10}$$

where l = orbital angular momentum
The equation above is simplified and the result is stated as:

$$\frac{d^2R}{dr^2} + \frac{2}{r}\frac{dR}{dr} + \left[k^2 - \frac{l(l+1)}{r^2}\right]R(r) = 0 \tag{1.11}$$

where $k = \frac{\sqrt{2\mu E}}{\hbar}$
Equation (1.11) is reminiscent of spherical Bessel differential equation. The solutions are the spherical Bessel function of order l, $j_l(kr)$ and the spherical Neumann function of order l, $n_l(kr)$. The general solution is:

$$R_{n,l}(r) = C_l j_l(kr) + D_l n_l(kr) \tag{1.12}$$

where C_l & D_l are constants.
The spherical Neumann function $n_l(kr)$ are discarded, since they are divergent at r=0[21]. Unlike the spherical Neumann function, the behavior of the Bessel function is such that it is finite at the origin. The finite requirement of the wave function suggest that D must be equal to zero. This reduces (1.12) to $R_{n,l}(r) = C_l j_l(kr)$. Applying boundary conditions, at $r = a$, $j_l(ka) = 0$. Let β_{nl} be the n^{th} zero of the spherical Bessel function of order l, thus $k_{nl} = \frac{\beta_{nl}}{a}$. Inserting this expression into (1.11), we get the allowed energy eigenvalues, which also represents the confinement energy.

$$E_{nl} = \frac{\hbar^2}{2\mu a^2}\beta_{nl}^2 \tag{1.13}$$

For the ground state ($n = 1, l = 0$), then $\beta_{1,0} = \pi$[21], hence the final form of the confinement energy of the quantum dots is:

$$\boxed{E_C = \frac{\pi^2\hbar^2}{2\mu a^2} = \frac{\pi^2\hbar^2}{2a^2}\left(\frac{1}{m_e^*} + \frac{1}{m_h^*}\right)} \tag{1.14}$$

Equation (1.14) represents the confinement energy of the QD, which is one of the important parameter to determine the band gap energy of the nanocrystal.

1.3.4.2 The Brus Equation

Brus gave the first theoretical calculation for semiconductor nanoparticles (using CdS and CdSe as examples) based on "effective mass approximation" (EMA)[17].

$$E_g^{QD} = E_g^{bulk} + \frac{\pi^2\hbar^2}{2\mu R^2} - 1.786\frac{e^2}{4\pi\epsilon_0\epsilon_r R} \tag{1.15}$$

where ϵ_r is the relative permittivity
Kayanuma accounted for the electron-hole spatial correlation effect[22] and modified the Brus Equation. Based on the modified equation, the size dependence on the band gap energy of quantum dots can be quantified as follows:

$$\boxed{E_g^{QD} = E_g^{bulk} + \frac{\pi^2\hbar^2}{2\mu R^2} - 1.786\frac{e^2}{4\pi\epsilon_0\epsilon_r R} - 0.248E_{Ry}^*} \tag{1.16}$$

The first term in the right hand side of Equation (1.16) represents the band gap energy of bulk materials, which is characteristic of the material. The second additive term of the equation represents the additional energy due to quantum confinement having a R^{-2} dependence on the band gap energy. It can indeed be thought of as the infinite spherical-well contribution to the band gap. The third subtractive term stands for the columbic interaction energy exciton having R^{-1} dependence (often neglected due to high dielectric constant of semiconductor material). The numerical factor in this term originates from calculations of wave function overlap integrals and its value may vary slightly from material to material. The last subtractive term, stands for spatial correlation effect (independent of radius) and significant only in case of semiconductor materials with low dielectric constant[17]. In general, the band gap energy of the QD is the contribution of the following parameters.

$$E_g^{QD} = E_g^{bulk} + E_{confinement} + E_{exciton} + E_{Rydberg}$$

1.4 Colloidal Quantum Dots

The distinction between atoms, molecules, quantum dots and bulk materials lie in their size and the number of atoms bound. QDs usually contain about 100-10000 atoms. It is clear that by binding more and more atoms together, the discrete energy levels of the atomic orbitals merge into continuous energy bands as it is apparent in the figure below[1].

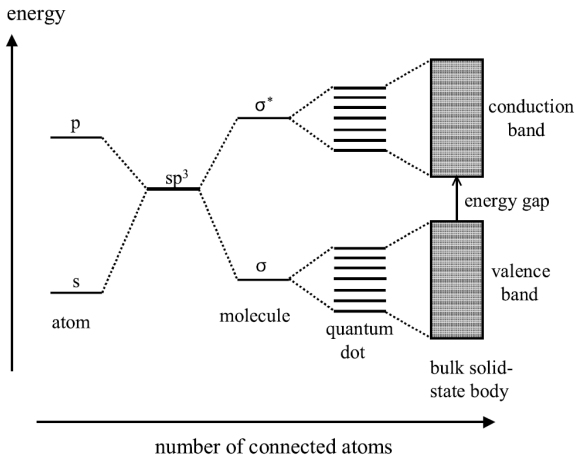

Figure 1.5: Electronic energy levels depending on the number of bound atoms[1]

Colloidal QDs differ remarkably from other QD systems such as self-assembled QDs and litographically defined QDs, as they are chemically synthesized using wet chemistry and are free-standing nanoparticles/nanocrystals grown in solution. In fabrication of CQDs, the reaction chamber contains a liquid mixture of the precursors and capping or complexing agent that control the nucleation and growth. The key parameter in the controlled growth of these nanocrystals is the presence of growth controlling agent as the nanoparticles have the tendency to aggregate and form large clumps, hence, a so called capping agent or complexing agent is required. Some commonly used inexpensive complexing agents include tartaric acid, trisodium citrate and ethanolamine can be utilised for synthesis of CQDs.
In this paper, trisodium citrate ($Na_3C_6H_5O_7$) was used to synthesize CdS CQDs using a modified version of chemical bath deposition technique illustrated by Fekadu *et al*[23].

1.5 Applications of Quantum Dots

Colloidal semiconductor quantum dots exhibit size-dependent optoelectronic properties, making them promising materials for many applications, such as solution processed solar cells [24]–[26], luminescent solar concentrators [24], photodetectors[27], light emitting devices[24], [28], optoelectronic devices[24], [29] and biomedical imaging[30]–[32].

The quantum cofinement effect in QDs has enabled the tunability property of the band gap of the semiconductor allowing easy manupilation of essential characteristics such as absorption, emission and conductivity of the material[33]. As a consequence, QDs have been incorporated as active elements in a wide variety of devices and applications.

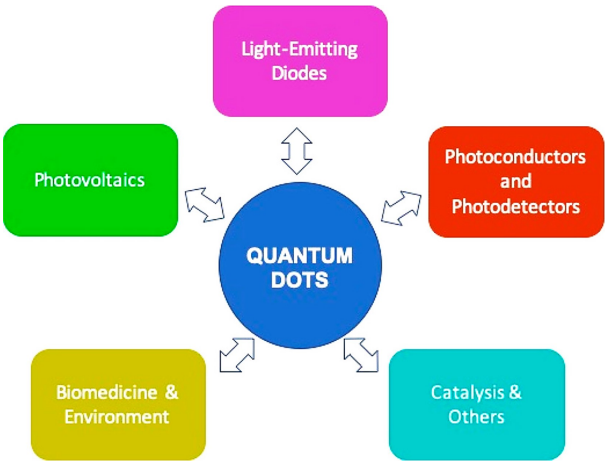

Figure 1.6: QD-based applications

Many of these applications are now commercially available and are incorporated into our daily life,such as the case of QD-based displays[34]. Despite now being part of mature technologies, QD synthesis, characterization, and applications still constitute a highly active field of investigations. While original QD research was heavily centered in group IV and III-V compounds,progress in the synthesis over the years has expanded the elemental composition[35]. Currently, QDs are also based on II-VI and I-III-VI compounds, as well as transition-metal dichalcogenides, perovskites, and carbon, among others. QD applications are mostly based on their exquisite optical properties and their role in light emission, conversion, and detection. As such, QDs encompass a large number of areas of application, as depicted in the figure above.

One of the most important areas of application of QDs is in photovoltaics due to the high renewable energy demand prevailing in the world. Devices for photovoltaics have long incorporated nanomaterials in order to boost the energy conversion efficiency[36]. Nevertheless, new strategies to accomplish that goal have been reported, including those involving CdS QDs[37] and CdSe and CdSe/CdS core-shell QDs[38]. Also, new methods for capping PbS QDs with atomic ligands[39] and improving passivation of CdSe/CdS/ZnS core-shell-shell QDs thin films have been described[40]. Ligand and solvent engineering were also applied in PbS QD films[41]; the latter were also studied in conjunction with ZnO films[42]. Homogeneous dispersion of core-shell CdS/ZnS QDs in copolymers was achieved using super critical carbon

dioxide synthesis[43]. Furthermore, theoretical studies by DFT calculations helped design CdSe and CdS QD-based materials for energy conversion applications.

1.6 Statement of the Problem

It has been reported in numerous literature that the optical and electrical properties of CdS thin films can be altered by doping it with metallic ions such as Mg^{2+}[44], Zn^{2+}[45], Cu^{2+}[46], Fe^{2+}[47], Co^{2+}[48] etc. having ionic radii smaller than that of the host ion Cd^{2+}. These dopant ions due to their smaller ionic radii diffuse well into the host CdS lattice enhancing its conductivity due to lattice unit cell compression. However, the effect of incorporation of dopant ions of greater ionic radii than that of Cd^{2+} on the optical, electrical and structural properties of CdS is still under investigation. Pb^{2+} is a heavy metal ion having ionic radius of 1.20Å, which is slightly higher than that of Cd^{2+} (0.97Å), and hence it is supposed that the lead ions can alter the properties of pure CdS.

Despite the promising potential of Pb-doped CdS CQDs, there is a noticeable gap in the existing literature regarding their comprehensive characterization and understanding. Limited work has been conducted to investigate the optical and electrical properties of Pb-doped CdS CQDs, specifically focusing on the Burstein-Moss effect. The Burstein-Moss effect, which involves the bandgap widening in heavily doped semiconductors, has been extensively studied in bulk and thin-film materials. However, its manifestation and implications in Pb-doped CdS CQDs have received scant attention. The lack of in-depth investigations on this particular system hinders the development of a comprehensive understanding of the Burstein-Moss effect in doped QDs and restricts their potential applications. Thus, this scientific work aims to shed light on the interplay between dopant concentration, bandgap widening, and the resulting changes in the optical and electrical behavior of the doped CQDs.

1.7 Research Objectives

The direct determination of the carrier concentration value in the conduction and valence band of doped QDs requires either theoretical model or computational study due to the quantum confinement effect present in these nanocrystals. However, by studying the optical and electrical properties of the doped samples obtained experimentally, we can infer whether there is an agreeing correlation showing that indeed an increase in dopant concentration can result in the Burstein-Moss effect or widening of bandgap. The general and specific objectives of this research are listed below:

1.7.1 General Objectives

The general objectives of this work is to investigate the doping effect of Pb atoms on the optical and electrical properties of CdS CQDs and bridge the research gap by conducting a systematic study on Pb-doped CdS CQDs. By thoroughly investigating the absorption spectra, photoluminescence properties, and electrical conductivity of the samples; the Burstein-Moss effect is examined. Additionally, the correlation between optical and electrical properties is investigated.

1.7.2 Specific Objectives

The specific objectives of this study are:

(i). To synthesize Pb-doped CdS CQDs using a modified chemical bath deposition technique.

(ii). To characterize the optical properties of Pb-doped CdS CQDs using UV-Vis, PL, and FTIR spectroscopies.

(iii). To explore the influence of Pb doping on the optical bandgap E_g and estimated particle size D of CdS CQDs in context to the Quantum Confinement and Burstein-Moss Effect.

(iv). To investigate the electrical properties of Pb-doped CdS CQDs, including resistivity and conductivity, in thin film form.

1.8 Significance of the Study

The significance of this study lies in its contribution to the limited body of knowledge on Pb-doped CdS CQDs, specifically in relation to the Burstein-Moss effect. The findings will not only enhance our understanding of the fundamental properties of doped QDs but also provide valuable insights for the development of novel optoelectronic devices. By addressing this research gap, this master's thesis aims to pave the way for future advancements and applications of Pb-doped CdS CQDs in various technological fields.

1.9 Structure of the Thesis

The thesis is structured as follows:
Chapter 1: *Introduction*; In this chapter, the background and significance of the study are presented, highlighting the research motivation and the objectives of the research. The

research questions to be addressed are identified, and important concepts in the study are outlined. Finally, the organization of the thesis is described.

Chapter 2: *Literature Review*; This chapter provides a comprehensive review of the relevant literature on the topic of interest. It covers the theoretical and conceptual foundations related to Pb-doped CdS CQDs, including their synthesis, characterization, and optical and electronic properties. The quantum confinement effect in QDs is explored, and previous studies on the effects of dopant concentration are critically analyzed. The chapter concludes by identifying the research gap that the current study aims to address.

Chapter 3: *Methodology of the Study*; In this chapter, the experimental methodology employed in the research is detailed. It includes a description of the materials and reagents used, the synthesis and doping procedures, and the characterization techniques employed to evaluate the optical and electrical properties of the Pb-doped CdS CQDs. The experimental setup, data analysis methods and parameters are also discussed.

Chapter 4: *Results and Discussion*; The results obtained from the experimental study are presented and analyzed in this chapter. The optical and electrical characterization data are discussed in relation to the dopant concentration variations. The observed trends and phenomena are interpreted, and their implications for the optical and electronic properties of the QDs are discussed. The findings are compared with the existing literature, and any discrepancies or novel insights are highlighted.

Chapter 5: *Conclusion*; The final chapter summarizes the main findings of the study and addresses the research questions posed in the introduction. The implications and significance of the results are discussed, and suggestions for future research directions are provided. The chapter concludes by highlighting the limitations of the current work and mentioning future prospective studies relevant to this research.

Chapter 2

Literature Review

2.1 Doping in Colloidal Quantum Dots

Colloidal quantum dots (CQDs) have emerged as a promising class of nanomaterials with unique size-dependent electronic and optical properties. These semiconductor nanoparticles exhibit quantum confinement effects, where the electronic structure and bandgap energy can be tuned by controlling their size[4]. However, to further enhance their performance and expand their applications, researchers have turned their attention to the process of doping. Doping involves introducing impurity atoms or molecules into the crystal lattice of QDs, altering their structural, electrical and optical properties. This deliberate incorporation of dopants allows for tailoring and fine-tuning of the QD properties, opening up new avenues for engineering their photophysical characteristics, charge transport behavior, and energy levels[5]. In this context, doping in CQDs has gained significant attention as a means to overcome limitations and unlock their full potential for various applications, including optoelectronics, photovoltaics, catalysis, and sensing.

Doping of CQDs like PbS, PbSe, and CdSe has been extensively studied for various applications. Researchers have explored different doping techniques to manipulate the optical, electric, and magnetic properties of CQDs. Methods such as photochemical doping have been used to introduce extra charge carriers into these nanoparticles, leading to improved functionalities[49]. Surface ligand engineering has emerged as an effective way to alter free carrier concentrations and doping types in CQDs, with halide-atomic ligands being popular for producing PbS QDs[50]. Additionally, the synergistic effect of PbS CQDs and bismuth telluride (Bi_2Te_3) has been leveraged to develop photodetectors capable of detecting mid-wave infrared bands, showcasing excellent performance and sensitivity[51]. Furthermore, the doping of CQDs is crucial for applications in photovoltaics, where alternative doping methods have been developed to promote efficient charge extraction in solar cells[52]. These studies collectively highlight the significance of doping in enhancing the properties and functionalities of CQDs for a wide range of applications.

2.2 Cadmium Sulfide Quantum Dots

Cadmium Sulfide (CdS) Quantum Dots are inorganic semiconductor nanocrystals belonging to cadmium chalcogenide (group II-IV) family which have size typically upto 5.8nm since the Bohr radius for CdS particles is around 5.8 nm[53]. CdS QDs have discrete energy levels hence show a 3D quantum confinement. While for bulk CdS there is continuous energy band, the CdS QDs have discrete energy levels. Band gap for bulk CdS is around 2.42eV while for CdS QD may be tuned varying from 2.42eV to 4.5eV[9]. Experimental investigations show that peak observed in UV-Vis absorption spectroscopy for bulk CdS is around 525-550 nm while for CdS QD may be observed around 375-425nm.
CdS QDs are synthesized in three different crystallite structures- face centered cell (fcc), hexagonal centered cell (hcp)[10] and cubic closed packing (ccp). CdS QDs can be synthesized by various different techniques like reverse micelle synthesis[54], microwave synthesis[55], chemical bath deposition[56], sol gel spin coating method[57] and wet chemical method[58]. There are myraids of applications of using CdS QDs such as in selective ion probes[59], nanotube array photoelectrodes[60], photocatalysis[61], bioapplications[62], quantum dot sensitized solar cells[63], light emitting diodes[64] etc...

2.3 Doping of CdS Quantum Dots

Doping of CdS quantum dots with various elements is an intriguing area of research that aims to modify and enhance the properties of these nanoscale semiconductors. As mentioned before, doping involves intentionally introducing impurities or foreign atoms into the crystal lattice of CdS QDs, which can profoundly influence their electronic, optical, and chemical characteristics. By carefully selecting the dopant elements, researchers can tailor the quantum dot's behavior to meet specific application requirements. Doping can lead to improved conductivity, enhanced emission properties, increased stability, and expanded functionality, opening up new avenues for applications in optoelectronics, solar cells, sensors, and more. The exploration of different dopants in CdS QDs offers exciting opportunities to push the boundaries of nanoscale engineering and create advanced materials with exceptional properties and performance.
Doping in CdS QDs involves the substitution of some of the Cd or S atoms within the crystal structure with dopant atoms, which can be elements from the periodic table. The choice of dopant elements is crucial, as it determines the resulting modifications in the quantum dot's electronic, optical, and chemical properties. By judiciously selecting dopants, researchers can control the band structure, energy levels, carrier dynamics, and surface chemistry of CdS

QDs.

One of the primary objectives of doping in CdS QDs is to enhance their electrical conductivity. Intrinsic CdS QDs are known for their limited conductivity due to the presence of surface traps and defects. However, by introducing suitable dopants, such as transition metals (e.g.,Zn, Mn, Fe, Ni) or rare earth metals (e.g., Eu, Gd), it is possible to improve the charge transport properties by creating additional energy levels within the bandgap of the QDs. These dopants act as shallow donors or acceptors, facilitating the movement of charge carriers and enhancing the overall conductivity of the nanomaterials.

Furthermore, doping can significantly influence the optical properties of CdS QDs, particularly their luminescence behavior. The emission properties of pristine CdS QDs can be tailored by incorporating dopants that introduce defect states or alter the surface chemistry. For example, rare-earth elements such as Eu or Tb can be doped into CdS QDs to achieve efficient and tunable luminescence in the visible or near-infrared regions of the electromagnetic spectrum. This ability to engineer the emission wavelength and intensity of QDs through doping has tremendous potential for applications in lighting, displays, biological imaging, and sensing.

Overall, the doping of CdS QDs with various elements holds great promise for the development of advanced nanomaterials with tailored properties and functionalities. By harnessing the unique characteristics of dopant elements, researchers can push the boundaries of CdS quantum dot applications, enabling advancements in fields such as optoelectronics, photovoltaics, chemical sensing, and biomedical imaging. Continued exploration and understanding of the doping process in CdS QDs will undoubtedly contribute to the design and synthesis of novel materials with enhanced performance and expanded technological applications.

The following papers are related to doping of CdS QDs using various transition metals and rare earth metals. This section highlights the versatility of CdS QDs as a host for different dopant species.

Poornaprakash *et al* (2019), have doped CdS QDs with a rare earth metal ions, *Gadolinium (III)* to study the influence on the structural, optical, magnetic and photocatalytic properties of the seniconductor nanocrystals. They have fabricated CdS, $Cd_{0.98}Gd_{0.02}S$ and $Cd_{0.96}Gd_{0.04}S$ by solvothermal method. The resulting QDs had spheroid shapes with sizes ranging from 3.8-6.2nm. The magnetic property analysis of the doped samples exhibited superparamagnetism. Moreover, the photocatalytic activity of all the three samples was studied on malachite green oxalate dye under artificial solar irradiation. After careful inspection, it was found that $Cd_{0.96}Gd_{0.04}S$ had better photocatalytic properties[65].

Ganguly and Nath (2020) have investigated effects of doping Manganese (Mn^{2+}) ions on CdS QDs to be used as sensitizers in solar cell. They prepared different concentrations of Mn^{2+} doped CdS QDs with poly-vinyl alcohol (PVA) capping layer via simple chemical method. The XRD showed that the prepared pure CdS and Mn doped CdS samples had similar crystal structure. The size of synthesized QDs were estimated to be around 6 nm from both XRD as well as UV–Vis absorption study. The presence of prominent peak of Mn^{2+} in the EDX pattern of CdS indicated successful doping of Mn in CdS QDs. Furthermore, the synthesized QDs were introduced as sensitizer in a ZnO thin film solar cell and the solar cell parameters were obtained for white light illuminated condition. The 2% Mn^{2+} doped CdS QDs on ZnO thin films exhibited the highest short-circuit current density (J_{SC}) of $5.2 mA/cm^2$, an open-circuit voltage (V_{OC}) of 0.6 V, a fill factor (FF) of 0.67 and a highest power conversion efficiency (η) of 2.09%. For higher doping concentrations it was revealed that the photo conversion efficiency decreased[66].

While the synthesised nanocrystals are not QDs, Shkir *et al* (2020), have done a research on the facile and cost-effective fabrication of CdS thin films with diverse contents of Zn carried out on substrates of glass maintained at $300°C$. The grown CdS films were observed to have monophasic hexagonal system at all Zn contents through structural and vibrational inspections. The values of crystallites size were determined in range of 16 to 31 nm. The existence of Zn and its homogeneity were confirmed by EDX and e-mapping. SEM study displayed the modification in surface topography of CdS films by Zn content. UV-Vis-near IR spectroscopy study revealed that the grown films were of good optical transparency. The indices of refraction values were estimated to be in range of 1 to 2.8 owing to Zn. The PL study proposed the applications of grown films in green LEDs as the emission peak has been observed at $513 \pm 17 nm$. Enhancement in optical limiting behaviour of CdS was also noticed when doped with Zn[67].

Muthusamy and Muthukumaran (2015) have inspected on undoped and Cu doped CdS thin films ($Cd_{1-x}Cu_xS$, x = 0, 0.02, 0.04, 0.06 and 0.08) deposited on glass substrate by chemical bath deposition (CBD) method at $80°C$ from aqueous solution. of the [$Cd_{1-x}Cu_xS$] films was studied by EDX analysis. The optical absorption and transmission studies revealed that [$Cd_{1-x}Cu_xS$] films had direct allowed transition with band gap energy increasing from 2.18 to 2.34 eV. The average crystalline size was calculated from X-ray line broadening and it had decreased from 3.09nm (CdS) to 2.81nm ($Cd_{0.96}Cu_{0.04}S$). The substitution of Cu concentrations into the Cd-S lattice was confirmed by the change in lattice parameters using FTIR and PL studies. The observed lower crystal size (2.81nm) and higher energy gap (2.28eV) of $Cd_{0.96}Cu_{0.04}S$ thin film was useful to design a suitable window material in fabrication for

solar cells[68].

Thambidurai *et al* (2011), have investigated on Ni-doped CdS QDs prepared by chemical precipitation technique. The XRD results indicated that the particle size of Ni-doped CdS QDs was smaller than that of undoped CdS and no secondary phase was observed. The average grain size of the QDs was found to lie in the range of 2.7-4nm. The compositional analysis results showed that Cd, Ni, and S were present in the samples. HRTEM studies revealed that the average particle size of undoped and Ni-doped CdS QDs was 2 and 3nm, respectively. The absorption edge of Ni-doped CdS nanoparticles was found to shift towards the higher-wavelength (red shift) side when compared to that of undoped CdS and the band gap was observed to lie in the range of 3.79-3.95 eV. They have attributed such increase in band gap than that of the bulk CdS to the quantum confinement effect present in CdS QDs[69].

Heiba *et al* (2019), have examined the effect of Vanadium (V) and Yttrium (Y) doping on the structural, optical and electronic properties of CdS. The Nano $[Cd_{1-x}Y_xS]$ and $[Cd_{1-x}V_xS]$ $(0 \leq x \leq 0.2)$ systems were formed by thermolysis procedure in the air at $220^{\circ}C$. Rietveld refinement of XRD data revealed that $Cd_{1-x}V_xS$ had two phases (cubic and hexagonal) and its cubic phase ratio increased with increasing the amount of V doping in the matrix. In case of Y-doped CdS, the system also had two phases but the cubic phase disappeared totally when the amount of doping was above 10%. UV-Vis spectroscopy revealed that the energy gap of CdS QDs (2.66 eV) had a blue shift and larger than bulk one (2.42 eV). Doped CdS with either V- or Y-doped CdS, decreased the energy gaps to 2.28 and 2.01 eV for $Cd_{0.8}Y_{0.2}S$ and $Cd_{0.8}V_{0.2}S$, respectively. Their analysis suggested that the doping ion plays an important role in tuning emission of CdS which can be used in several applications such as biological sensors and photodetectors[70].

Thambidurai *et al* (2010), have done studies on optical absorption and structural properties of Fe doped CdS QDs. The samples were prepared by chemical precipitation technique. Two main peaks of Raman spectra were present at 300 and $601cm^{-1}$, which were respectively, specified as the fundamental modes. The LO peaks of the Raman spectra of the CdS QDs show red shift on Fe doping. The HRTEM image revealed that undoped and Fe doped CdS QDs had particle size lying in the range of 2-3 nm. The optical absorption spectra of the samples showed that the absorption edge was located at around 330-380 nm, which is blue shifted when compared to that of bulk CdS (512 nm). They have pointed out that such blue shifting was due to the quantum size confinement effect. Lastly, they have concluded that the optical band gap of nanocrystalline CdS was observed to decrease on Fe doping[71].

Maity *et al* (2021), have investigated the role of Cobalt doping in CdS QDs for potential ap-

plication in thin film optoelectronic devices. The synthesized $Cd_{1-x}Co_xS$ (where $0 \leq x \leq 0.08$) QDs, showed the cubic zinc blende structure with no impurity phase. The crystallite size estimated by XRD and TEM measurements was around 2 nm. The XPS spectra revealed the electronic structure of the CdS and 6% Co-doped CdS QDs. From the XANES analysis, it was estimated that the oxidation state of Cd atoms was +2 in all the samples. EXAFS measurements showed that there was no change in the crystal structure with increasing Co-doping concentration. The Raman intensity was found to decrease and the FWHM increased with the Co concentration due to local structural disorder as a result of doping. The band gaps estimated by Tauc's plot showed the linear decrease with the doping concentration. The photocurrent obtained from thin film heterojunction with 8% Co-doped CdS QDs was 0.811 mA at -10 V applied voltage[72].

Firdous *et al* (2013), have explored effect of Ni-doped CdS synthesized through chemical precipitation method using a high-boiling solvent. The mean crystal size obtained by FWHM analysis was 3.33 nm for CdS, 3.37 nm for CdS:Ni (2 mM) and 3.39 nm for CdS:Ni (4 mM). Furthermore, the electrical conductivity data revealed the semiconducting behaviour of both pure CdS and Ni-doped CdS QDs. The optical absorption analysis conducted in UV-vis range 200-900 nm revealed the transparency of these QDs in the entire visible range but not in UV range. The results based on optical analysis yielded band gap values of 2.65 eV for CdS, 2.59 eV for CdS:Ni (2 mM) and 2.53 eV for CdS:Ni (4 mM) QDs. As a result they have surmised that the pure CdS and Ni-doped CdS were blue shifted with respect to the bulk CdS (2.42 eV) due to the quantum confinement effect; however, Ni-doped CdS QDs were red shifted with respect to pure CdS nanocrystals[73].

Tan *et al* (2020), have worked on Eu-doped CdS QDs with Eu^{3+} concentration in the range of 0.5-10%. The samples were successfully synthesized by wet chemical method. Doping Eu^{3+} ions did not change the zinc blende crystal structure of CdS QDs but its lattice constant decreased slightly with increasing dopant concentration. For the dopant concentration of about 7.0 mol%, $CdS:Eu^{3+}$ QDs yielded the maximum efficiency of red emission. They have showed that energy transfer from CdS lattice to Eu^{3+} ions takes place via the exchange interaction mechanism. In this process, the energy transfer efficiency increases with an increase of Eu^{3+} concentration. By using the Inokuti-Hirayama model, the dominant interaction mechanism between Eu3+ ions was found to be dipole–dipole interaction[74].

2.4 Lead (*Pb*)-doped CdS Quantum dots

Pb (lead) doping of CdS QDs has emerged as a fascinating area of research with significant potential to enhance the properties and expand the applications of these nanomaterials. CdS QDs are semiconductor nanoparticles that exhibit unique size-dependent properties, including tunable bandgap, high PL quantum yield, and efficient charge carrier dynamics. The incorporation of Pb dopants into CdS QDs offers opportunities to further manipulate and optimize their optical, electrical, and structural characteristics, leading to advancements in fields such as optoelectronics, photovoltaics, sensing, and more.

Bhanu *et al* (2021), have investigated the photocatalytic activity of heavy metal (Pb, Ag and Sn) doped CdS QDs synthesized using Ocimum Sanctum leaf extract used as capping and reducing agent. They have mainly highlighted the implementation of green co-precipitation synthesis mechanism in fabrication of QDs. They have mentioned that the CdS nanocrystals are very promising in photocatalysis due to their unique optical and photocatalytic properties. A wide forbidden band of 2.42 eV of CdS nanocrystals is very desirable for photocatalysis driven by visible light. Added to this, high specific surface area to volume ratio, high crystallinity, short bulk to surface diffusion, and exciton stability are some of the advantages of CdS QDs in visible light-driven photocatalysis. Among the three implemented dopants (Pb^{2+}, Ag^{+} and Sn^{2+}), Pb doped CdS QDs with band gap of 2.03 eV showed superior photocatalytic efficacy with degradation efficiency of 98.01% which further strengthens the use of lead atoms as dopants in CdS QDs[75].

Veerathangam *et al* (2018) have researched the photovoltaic performance of Pb-doped CdS QDs for solar cell application. They have employed the successive ionic layer adsorption and reaction (SILAR) method to deposit the undoped CdS and Pb-doped CdS QDs with different doping concentrations over the TiO_2 nanostructures. The systematic investigations of photoanode were carried out and the observed results revealed that the deposited sensitized layer had a spherical morphology. Polycrystalline nature of the deposited film was observed, but the characteristic peaks for Pb or PbS were not present. However, the presence of lead was confirmed through EDX and elemental mapping study. The superior optical absorption and photovoltaic performance were observed in the 2% Pb-doped CdS QDs sensitized cell. The corresponding cell parameter values such as η, J_{sc}, V_{oc} and FF were 1.19%, 3.76 mA/cm^2, 0.61 V and 51.5% respectively[76].

Yuan *et al* (2016), have worked on improving the photocurrent in QDSSCs by employing ternary alloy $Pb_xCd_{1-x}S$ QDs as photosensitizers. Their work was motivated by the fact that, while PbS quantum dots (QDs) have been successfully applied in heterojunction so-

lar cells, showing remarkable conversion efficiency, corresponding PbS QDSSCs still have shown low device performance. Therefore, one way to improve such QDSSCs and utilize the high underlying quantum efficiency was alloying other metals to give a higher quality QDs. The ternary alloy was synthesised using SILAR mechanism. Firstly, they found that the three-SILAR-cycle ($Pb_{0.54}Cd_{0.46}S$) presented a much higher photocurrent compared to PbS and CdS. Then, by investigation of the absorption spectrum, cyclic voltammogram (CV), and dark I-V current of five-SILAR-cycle QDs, it was suggested that $Pb_xCd_{1-x}S$ QDs had a wider absorption range compared to the CdS QDs and a higher conduction band edge and reduced trap density compared to the PbS QDs. This indicated that the ternary alloy has the potential to overcome the shortcomings of CdS and PbS for QDSSC applications. Furthermore, by comparing the ($Pb_{0.54}Cd_{0.46}S$), ($Pb_{0.31}Cd_{0.69}S$), and ($Pb_{0.24}Cd_{0.76}S$) QDSSCs, they found that the ($Pb_{0.54}Cd_{0.46}S$) solar cell presented a significant J_{sc}, up to 20 mA/cm^2, by the optimization of the SILAR cycles. Finally, a coating layer of CdS deposited onto ($Pb_xCd_{1-x}S$) photoelectrode gave enhancements in the photocurrent to 22.6 mA/cm^2 and in the efficiency to 3.2%[77].

Guglielmi *et al* (1998), have studied the optical and structural properties of Hg:CdS and Pb:CdS nanocrystals. They have mentioned that undoped CdS QDs were not the best choice for devices intended for telecommunication purposes, as it has its bulk absorption band at 510 nm. Hence, they have chosen Hg and Pb as prime candidates as dopant species due to their smaller band gaps and absorption bands located in the near-infrared, at about 2500 and 3350 nm, respectively. Furthermore, both these sulfides have a Bohr radius which is larger than that of CdS and should have enhanced non-linearity effects. In principle, they have fabricated so called binary system of $Hg_xCd_{1-x}S$ and $Pb_xCd_{1-x}S$ to adjust the absorption wavelength by varying the composition of the components with $0 \leq x \leq 1$. Finally, they have prepared thin glass-like films with a mixture of the colloidal sol and an alkoxide solution to study the non-linear optical effects. The $Pb_xCd_{1-x}S$ binary system showed non-linear properties at $1.064\mu m$ while the $Hg_xCd_{1-x}S$ lacked thermal stability. They have summarised that further investigation is required to derive clear cut conclusion for the study of the non-linear properties in such binary systems[78].

While the field of doping CdS QDs with various elements has seen substantial research activity, comparatively little investigation has been conducted specifically on Pb-doped CdS QDs especially with respect to Burstein-Moss Effect. Despite the significant potential offered by Pb as a dopant element, its utilization in CdS QDs remains relatively unexplored. The limited research on Pb-doped CdS QDs implies a gap in knowledge and understanding regarding the effects and applications of this specific doping combination. Therefore, there is an opportunity for researchers to delve deeper into this uncharted territory, unraveling the

unique properties and unlocking the untapped potential of Pb-doped CdS QDs.

Chapter 3

Methodology and Characterizations

3.1 Chemical Bath Deposition

Chemical bath deposition (CBD) is a widely used method for synthesizing metal oxide nanostructures and thin films due to its simplicity, cost-effectiveness, and versatility[79]–[81]. CBD involves the deposition of films using sparingly soluble metal salts and desired solutes, leading to the growth of well-aligned crystallites with enhanced grain structure. This method has been applied to various substrates such as glass, metal foams, and conductive oxides like FTO and ITO forming thin films[82], [83]. CBD has significantly contributed to the fabrication of semiconducting thin films for applications in sensors, optical devices, solar cells, photovoltaic modules, supercapacitors, transistors, and gas sensors[80], [84]–[86]. The technique's success lies in its ease of implementation, chemical processes control, and the ability to achieve high material deposition control. Additionally, advancements in CBD methods have led to innovations like protection layers to prevent unwanted depositions and improve production efficiency [87].

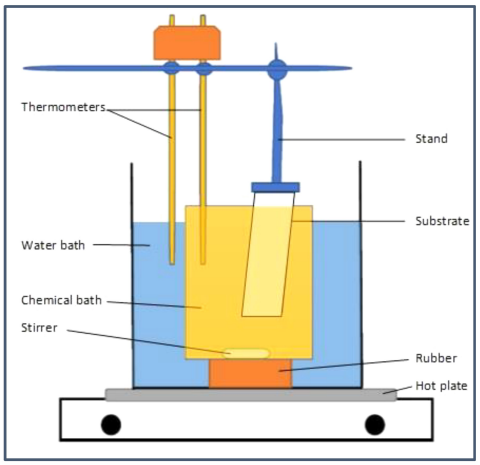

Figure 3.1: Typical CBD Setup

In this work, a modified version of the CBD technique based on Fekadu *et al*[23] was implemented for the synthesis of CdS CQDs and the Pb-doped samples. The CBD method is a widely used and cost-effective approach for the fabrication of CQDs. However, to incor-

porate Pb dopants into the host crystal lattice and achieve precise control over the doping concentration, modifications were made to the traditional synthesis procedure. The modified technique allowed for the successful incorporation of Pb dopants into the CdS QDs, enabling the investigation of the quantum confinement effects induced by Pb doping. The synthesis process was carefully optimized to ensure the reproducibility and quality of the Pb-doped CdS QDs, laying the foundation for subsequent characterization and analysis of their electronic and optical properties. In this modification, the glass substrate was removed since the final product is in colloidal form. Hence, no deposition was made onto a glass substrate, however, the principles behind the traditional CBD methods were used to prepare the colloidal samples.

Principles of CBD

The basic working principle behind the CBD process is similar to those for all precipitation reactions and it is based on relative solubility of the product. At a given temperature when the ionic product (IP) of reactants exceeds the solubility product (K_{SP}), precipitation occurs. Whereas if the ionic product is less than the solubility product, then the solid phase produced will dissolve back to the solution resulting in no net precipitation[88]. A central concept necessary to understanding the mechanisms of CBD is that of the solubility product (K_{SP})[23]. Given the chemical reaction:

$$M_a X_b \rightleftharpoons aM^{n+} + bX^{m-} \tag{3.1}$$

The solubility product (K_{SP}) is determined as:

$$K_{SP} = [M^{n+}]^a [X^{m-}]^b \tag{3.2}$$

$[M^{n+}]^a [X^{m-}]^b$ is called the ionic product. The solubility product (K_{SP}) highly depends up on temperature since almost all CBD reactions are carried out in aqueous solutions, the pH of the deposition solution will give the concentration of OH^- ions in the solution. When the solution is saturated, the ionic product is equal to the solubility product. But when the ionic product exceeds the solubility product the solution is supersaturated hence, precipitation occurs and ions combine on the substrate and in the solution to form nuclei. The more soluble the salt is, the greater the ion product and the greater is (K_{SP}) . However, (K_{SP}) also depends on the number of ions involved[79].

3.2 Parameters Affecting CBD

In the process of CBD, various parameters play crucial roles in determining the properties and characteristics of the deposited materials. Understanding and controlling these parameters is essential for achieving desired film quality, thickness, composition, and morphology. Factors such as reaction temperature, complexing agent, precursor concentration, deposition time, pH of the bath solution, and the presence of additives/dopants can significantly influence the growth kinetics, crystallinity, surface morphology, and optical and electrical properties of the deposited films. By carefully manipulating and optimizing these parameters, researchers can tailor the properties of CBD-deposited materials to meet specific application requirements.

Complexing Agent

Most CBD reactions are carried out in alkaline solution. To prevent precipitation of metal hydroxides, a complexing agent (often called a ligand) is added. The complexant also can reduce the concentration of free metal ions, which helps to prevent rapid bulk precipitation of the desired product. Therefore, such chemicals can act as both complexing and reducing agents. Ammonia is common complexing agent and pH controller, by adding some amount of ammonia in the alkaline solution we can control the rate of precipitation of metal hydroxide. The amount of ammonia to be added can be determined by calculating the stability constant between ammonia and soluble material. In this paper, trisodium citrate ($Na_3C_6H_5O_7$) was used as a complexing agent preventing the spontaneous aggregation and clumping of the CdS nanoparticles thus promoting stability, on the otherhand, aqueous ammonia was used as pH controlling agent.

Temperature, pH and Deposition Time

The parameters temperature, pH, and deposition time play critical roles in determining the properties and characteristics of the deposited material. In the CBD process, temperature affects the reaction kinetics and crystal growth rate. Higher temperatures generally lead to faster deposition rates and larger crystal sizes, while lower temperatures may result in slower growth and smaller crystals. The choice of pH in the deposition solution influences the solubility of the precursor compounds and the formation of desired products. Varying the pH can alter the reaction rates, control the morphology, and affect the composition of the deposited material. Additionally, the deposition time determines the thickness and coverage of the film or nanostructure. Longer deposition times typically lead to thicker layers, but there is a limit beyond which further growth may not significantly impact the properties. All three

parameters have effect on the optical, structural, electrical and morphological properties of the synthesized film[89].

3.3 Optical Study Parameters

The demand for optical characterization methods for material analysis and real-time monitoring or control applications has grown due to rapid advancements in semiconductor manufacturing and related technologies[90]. The optical characteristics of semiconductors encompass a range of properties related to the interaction between the semiconductor and electromagnetic radiation, such as absorption, diffraction, polarization, reflection, refraction, and scattering effects. By examining the electromagnetic spectrum, we can gain insights into the types of measurements and physical processes associated with different areas of interest regarding the optical properties of semiconductors (Bass, 1995). The optical properties of semiconductor nanoparticles are found to be extremely sensitive to the presence of excess charges. These charges can be generated by means of photo-excitation, chemically, i.e. by the direct reaction with strong reduction agents, by means of electrochemical charge transfer via an electrode or through doping. The induced changes in the optics can therefore be probed by means of various spectroscopy and the results obtained often provide detailed insights into the electronic structure of the investigated system[91].

Absorption and Emission

Optical studies involving absorption and emission in QDs are essential for understanding their unique electronic and photophysical properties. The two most common characterization methods are the UV-Vis and PL spectroscopy. UV-Vis spectroscopy reveals the energy levels at which QDs can absorb photons, providing insights into their size-dependent bandgap and quantum confinement effects. PL emission spectroscopy investigates the light emitted by QDs following excitation, offering valuable information about their electronic structure, emission wavelength, and radiative efficiency.

More specifically, UV-Vis spectroscopy measures the absorption of light in the ultraviolet (UV) and visible (Vis) regions of the electromagnetic spectrum. By analyzing the absorption spectrum, researchers can determine the energy levels at which a material absorbs photons, providing insights into its electronic structure and bandgap. In the context of QDs, UV-Vis spectroscopy helps to understand the size-dependent absorption properties and quantum confinement effects. As the size of QDs decreases, their bandgap increases, resulting in a blue-shift in the absorption spectrum.

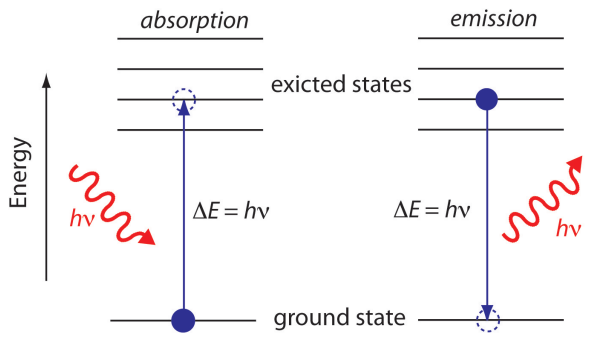

Figure 3.2: Absorption and Emission Processes in Semiconductors

PL spectroscopy, on the other hand, focuses on the emission of light from a material upon excitation. In this characterization method, a material is excited with photons of a specific energy, and the resulting emitted light is measured. In the case of QDs, when they absorb photons with energy greater than the bandgap, the electron is excited to the conduction band leaving the hole at the valence band. This results in the formation of an electrically neutral quasi-particle called exciton. These two opposite charges held by coulombic attraction can undergo radiative recombination, emitting photons of a specific wavelength. The PL spectrum reveals the energy distribution of the emitted photons and provides insights into the electronic structure, energy levels, and radiative properties of QDs. When a semiconductor is doped with donor impurities for n-type conductivity, the introduced impurity atoms have extra valence electrons compared to the host semiconductor atoms. These extra electrons become free or mobile within the material, increasing the concentration of negatively charged carriers.

In terms of PL study, n-type doping can have several effects on the emission properties of the material such as changes in absorption where the presence of donor impurities introduces energy levels within the bandgap of the semiconductor. These energy levels are typically closer to the conduction band. As a result, the doped material can efficiently absorb photons with energies corresponding to the bandgap. Secondly, augmented radiative recombination where excess electrons in CB can recombine with holes in VB and emit photon resulting in more intense PL signal. Thirdly, shifted emission wavelength, where the introduction of donor impurities can create additional energy levels within the bandgap of the semiconductor. These energy levels, known as donor levels, can influence the energy at which the electrons recombine with holes and emit photons

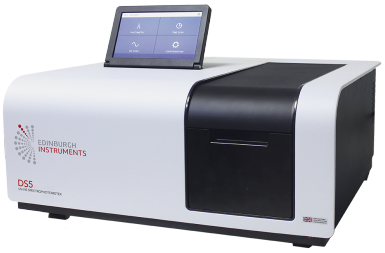

Figure 3.3: DS5 Dual Beam UV-Vis Spectrophotometer

Fourier Transform Infrared Spectroscopy

Fourier Transform Infrared Spectroscopy or FTIR is a widely used technique for analyzing the infrared absorption or transmission of a material. In FTIR spectroscopy, a broad range of infrared wavelengths is used to probe the molecular vibrations of a sample. The resulting spectrum provides information about the functional groups and chemical bonds present in the material. The FTIR spectrum is typically divided into three main regions:
The functional group region of the FTIR spectrum which corresponds to the higher wavenumber range, typically from 4000 to 1500 cm^{-1}. In this region, the infrared absorption bands are primarily associated with the vibrations of functional groups, such as hydroxyl groups (O-H), carbonyl groups (C=O), amines (N-H), and others. Secondly, the finger print region, also known as the mid-infrared region, which ranges from approximately 1500 to 500 cm^{-1}. This region contains a complex set of absorption bands that are highly specific to the molecular structure of the sample. It provides a unique "fingerprint" or characteristic pattern for the identification and differentiation of different compounds. Lastly, the region of low energy, also referred to as the far-infrared region or the "Reststrahlen" region, extends from approximately 500 to 10 cm^{-1}. In this region, the absorption bands are associated with collective vibrations of the crystal lattice, such as lattice vibrations, phonons, and other solid-state effects. This region is often used in the study of materials with specific crystal structures, such as minerals, polymers, and inorganic compounds[92].

Figure 3.4: The PerkinElmer Spectrum 65 FT-IR Spectrometer

In this study of the colloidal samples, the Spectrum 65 FT-IR, PerkinElmer was used, in the range 4000-400 cm^{-1}, resolution: 4 cm^{-1}, number of scans:4 in ATR mode.

Bandgap Determination

The results from the UV-Vis spectroscopy measured by the DS5 Dual Beam UV-Vis Spectrophotometer (Fig. 3.3), provide the amount of absorbed light as a function of the wavelength. By applying Beer-Lambert Law we can determine the absorption coefficient corresponding to given absorption.

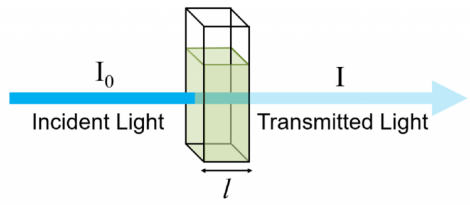

Figure 3.5: Light passing through a sample in cuvette

The relation for Beer-Lambert Law when light passes through the cuvette in Fig 3.5 is:

$$I = I_0 e^{-\alpha l} \tag{3.3}$$

where I is the intensity of transmitted light, I_0 is the intensity of incident light and α is the absorption coefficient
After a bit of algebraic manipulation we have the following relation between α and Absorbance:

$$\alpha = 2.303\frac{A}{l} = 2.303 A cm^{-1} \tag{3.4}$$

Where the standard dimensions of a cuvette is $l = 1cm$

Moreover, from Planck's Quantum Theory of light we have $E = h\nu$, further expanding this equation using the fact that $c = \nu\lambda$, we can determine a relation between the energy E and wavelength λ.

$$E = h\nu = \frac{hc}{\lambda} = \frac{6.625 \times 10^{-34} Js \times 2.998 \times 10^{8} m/s}{\lambda(m)} \tag{3.5}$$

Since $1eV = 1.602 \times 10^{-19} J$

$$E = \frac{1.986 \times 10^{-25} eV.m}{\lambda(m) \times 1.602 \times 10^{-19}} = \frac{1240 \times 10^{-9} eV.m}{\lambda(m)} \tag{3.6}$$

$$E = \frac{1240(eV.nm)}{\lambda(nm)} \tag{3.7}$$

Finally, the bandgap energy of the CQDs is calculated using the Tauc's relation:

$$(\alpha h\nu)^n = K(h\nu - E_g) \tag{3.8}$$

where K is a constant, and the exponent n assumes the values 2, 1/2 ,2/3 and 1/3 for direct allowed, indirect allowed, direct forbidden and indirect forbidden transitions, respectively. Since CdS is a direct bandgap semiconductor, the energy bandgap can be obtained by extrapolating the linear portion of $(\alpha h\nu)^2$ versus $h\nu$ to the energy axis at $(\alpha h\nu)^2 = 0$.

Particle Size Estimation using EMA

The particle size R of the CQDs can be estimated using eq. 1.16 by first determining the bandgap of the QDs E_g^{QD} using eq. 3.8. Since the dielectric constant of CdS nanoparticles is high ($\epsilon_r = 8.9$), the third subtractive term in eq. 1.16 can be neglected(P. Ghosh, 2015). Additionally, $E_{Rydberg}$ can also be omitted since it is only significant in case of semiconductor materials with low dielectric constant[17]. Following these, the estimation of particle size is affected by the the bandgap of the bulk semiconductor, the bandgap of the QD and confinement energy, $E_{confinement}$.

$$E_g^{QD} = E_g^{bulk} + \frac{\pi^2\hbar^2}{2\mu R^2} \tag{3.9}$$

Rearranging this to determine R, we have:

$$R^2 = \frac{\pi^2\hbar^2}{2\mu(E_g^{QD} - E_g^{bulk})} \tag{3.10}$$

where $\mu = \frac{0.211 \times 0.8}{0.211+0.8} m_0 = 0.167 m_0$, m_0 is the electron mass

Refractive Index, Dielectric Constant and Linear Optical Susceptibility

Refractive index (n) is one of the important optical parameters of semiconductor materials. In the present work it was estimated from the well known empirical relations given in Eqs 3.11-3.14. These mathematical approaches are broadly used for different groups of semiconductors for a wide range of optical band gaps. A suitable design of optoelectronic device needs a precise information of refractive indices of the materials. Refractive index is closely related to the electronic properties and band structure of the material. The following relations were used to estimate the refractive indices of the Pb-doped CdS CQDs[93].

⋆ Herve' and Vandamme Relation[94]:

$$n^2 = 1 + \left(\frac{A}{E_g + B}\right)^2 \tag{3.11}$$

where A=13.6eV and B=3.4eV

⋆Ravindra Relation[95]:

$$n = 4.084 + \varphi E_g \tag{3.12}$$

where $\varphi = -0.62 eV^{-1}$

⋆Tripathy Relation[96]:

$$n = n_0 \left[1 + \alpha e^{-\beta E_g}\right] \tag{3.13}$$

where $n_0 = 1.73$, $\alpha = 1.9017$, and $\beta = 0.539 eV^{-1}$

⋆Moss Relation[97]:

$$n^4 E_g = 95 eV \tag{3.14}$$

Following the determination of the refractive indices of the doped samples using the above relations, the dielectric constant (ϵ_r) and the linear optical susceptibility (χ) can be determined using the following expressions:

$$\epsilon_r = n^2 \tag{3.15}$$

$$\chi = \epsilon_r - 1 \tag{3.16}$$

These optical parameters were employed to study the Pb doping effect on CdS QDs due to their convenient relation with the optical bandgap and particle size. Moreover, the optical parameters can provide indirect information about the particle size of the QDs. The absorption and emission properties are influenced by the confinement of charge carriers within the QDs,

which is highly dependent on the QD size. Therefore, by analyzing the optical parameters, the influence of Pb doping on the particle size distribution of the CdS QDs can be investigated. Overall, these parameters provide a convenient and informative means to assess changes in the optical properties, band structure, and particle size distribution of the doped QDs.

3.4 Electrical Study

The electrical properties of the synthesized Pb-doped CdS CQDs were investigated by first preparing a thin film on an indium tin oxide (ITO) etched glass substrate. The colloidal samples were drop-casted then annealed at 130°C for 60min on a hot plate. Then aluminum was then deposited onto the substrate using Edwards Auto 306 vacuum pump/thermal evaporator. Following the deposition of Al, the IV charateristics of the samples were measured using the Keithley Source meter. (Fig. 3.6).

The conductivity of the thin films was determined by using the following relation:

$$\sigma = G\frac{L}{A} \tag{3.17}$$

where G is the conductance, which can be calculated from the slopes of dark J-V curves, L and A are the film thickness (40 nm) and area ($0.04cm^2$) of the thin films respectively.

Figure 3.6: Keithley 2400 SourceMeter

The Burstein-Moss Effect

The Burstein-Moss effect is the observable widening of the optical band gap of a semiconductor caused by increasing the dopant concentration within the semiconducting material. The effect was initially described by Tanenbaum and Briggs for InSb and later independently explained by Burstein and Moss[91].

As a result of the very large increase in the doping density the semiconductor is driven into degeneracy. This results in the Fermi level E_F, which is usually located within the band gap, being shifted into the majority carrier band. At moderate doping densities the dopant atoms contribute a moderate number of charge carriers to the respective bands and therefore the Fermi level is located somewhat below the conduction band edge for an n-type semiconductor and somewhat above the valence band edge for a p-type semiconductor. As more dopants

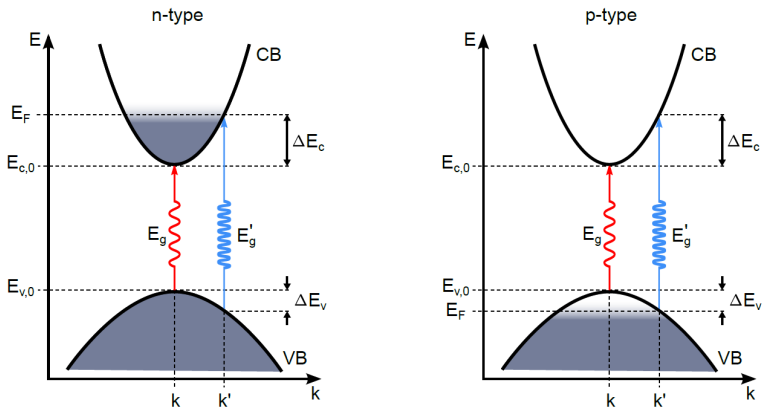

Figure 3.7: Schematic of the absorption edge shift in the energy-momentum diagram for the case of degenerate n-type and p-type semiconductors with the relevant energy levels marked[91]

contribute charge carriers to the bands the states in the proximity of the respective band edge become progressively populated. The amount by which the optical band gap increases is the so called Burstein-Moss shift (BM shift)[91].

The parabolic band approximation model is commonly used to describe the electronic structure of bulk semiconductors, where the dispersion of energy bands near the band edges is assumed to be parabolic. In the range where the widening of the optical band gap occurs due to the Burstein-Moss effect the measured optical band gap, E_m, is the sum of the optical gap of the as-synthesized material, E_0, plus that due to the filling of the conduction band caused by donors, ΔE_{BM}:

$$E_m = E_0 + \Delta E_{BM} \tag{3.18}$$

In semiconductor where a parabolic band is assumed, the band gap energy shift (ΔE_{BM}) due to the Burstein-Moss effect is related to the carrier concentration, n, according to the following:

$$\Delta E_{BM} = \frac{\hbar^2}{2m^*}(3\pi^2 n)^{2/3} \tag{3.19}$$

where $\hbar$ is reduced Planck's constant and m^* is the effective mass of the electron.

The increase in the optical band gap with increasing carrier concentration is related to the rise of the Fermi level in the conduction band of a degenerate semiconductor[98]. However, this model is not directly applicable to QDs due to their nanoscale size and quantum confinement effects resulting in a non-parabolic density of states. Nonetheless, we can still apply the concepts of BM sihft to doped QDs.

3.5 Experimental Procedure

One of the objectives of this paper is to utilise low cost and environmentally friendly mechanism of synthesizing QDs. As such, chemical bath deposition was found to be an effective and easily applicable method for obtaining good quality colloidal nanoparticles. Additionally, the use of trisodium citrate as a complexing agent promotes green synthesis since it is employed as food preservative and flavour enhancer in food engineering. As mentioned previously, CdS CQDs were prepared using modified chemical bath deposition. The experimental route began by preparing respective stock solutions of the precursors as follows:

- 100mL of 0.25M Cadmium Acetate dihydrate [$Cd(CH_3COO)_2 \cdot 2H_2O$]
- 100mL of 0.25M Thiourea [$CS(NH_2)_2$]
- 50mL of 1M TriSodium Citrate (TSC) [$Na_3C_6H_5O_7$]
- 20mL of 0.25M Lead Acetate trihydrate [$Pb(CH_3COO)_2 \cdot 3H_2O$]

Following the preparation of the stock solutions, the reaction vessels, beakers, pipettes and stir bar were dipped into hydrochloric acid (HCl) to avoid contamination. 250mL water used as a bath was poured in 1000mL beaker. The beaker was placed onto the hotplate set at $70°C$. A thermometer was placed inside the water bath to monitor its temperature. Another magnetic stirrer at room temperature was set to 400rpm for the preparation of the CdS CQDs. In a 100mL beaker with a stir bar placed at the stirrer, 10mL cadmium precursor was poured in from the stock solution followed by 10mL of distilled water (DW), then 5mL of trisodium citrate was slowly added into the beaker resulting in a white milky solution. However, this white cloudy solution turned clear in a few seconds. The complexing agent was followed by addition of 5mL of DW. Afterwards, 2mL of 30% aqueous ammonia (NH_3) was added drop-wise into the solution for setting the pH to around 9.5. Again 10mL of DW was added. Subsequently, 10mL of the sulfur precursor was poured in slowly and finally 8mL of DW was added and then the beaker was placed into the water bath @$70 \pm 1°C$ and 400rpm. The solution kept on stirring for 60min resulting in the formation of the CdS CQDs.

Preparation of the Pb-Doped CdS CQDs Samples

For the doped CQDs, similar procedure was applied except the Pb precursor was added into the solution. 0.10%, 0.15%, 0.20% and 0.25% of 10mL volume percentages were added to have the respective doping amounts. The doped samples hence contained a total sum of 10mL of Cd and Pb precursor. For instance, to prepare the 0.10% Pb-doped CdS sample, 9.99mL

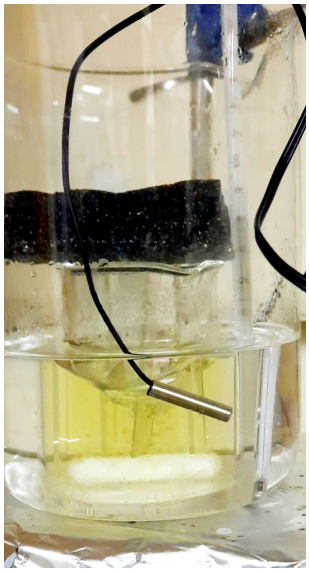

(a)

(b)

Figure 3.8: **(a)**CBD process for the synthesis of CdS Colloidal Quantum Dots [*The black wire is a thermocouple connected to digital thermometer*] **(b)**As-prepared Pure CdS Colloidal Quantum Dots

of Cd precursor was added into a 100mL beaker followed by 5mL DW then 10μL of the Pb precurosor was poured in followed by 5mL of DW. Consequently, the rest of the procedure follows the one described above. For each scenario, the Pb precursor was added using a pipette.

Reaction Mechanism

The reaction process for the formation of the CdS CQDs may be described by the following steps:

$$Cd(CH_3COO)_2 \cdot 2H_2O(aq) + TSC \rightarrow [Cd/TSC]^{2+}complex + 2CH_3COO^- + 2H_2O$$

$$[Cd/TriSodiumCitrate]^{2+}complex \xrightarrow{\text{hydrolysis}} Cd^{2+} + TriSodiumCitrate$$

$$Cd^{2+} + 4NH_3 \rightarrow Cd(NH_3)_4^{2+}$$

$$NH_3 + H_2O \rightarrow NH_4^+ + OH^-$$

$$CS(NH_2)_2 + 2OH^- \rightarrow S^{2-} + C(NH)_2 + 2H_2O$$

$$Cd(NH_3)_4^{2+} + S^{2-} \rightarrow CdS + 4NH_3$$

Trisodium citrate was used to limit the hydrolysis of the metal ion and impart some stability to the QDs and prevent aggregation or precipitation. Upon hydrolysis of the cation complex (step 2), the white milky solution turns colorless. As we can see in the last step of the chemical reaction, ammonia appears as a by-product in the reaction, however, due to the high volatile nature of ammonia it evaporates and the solution is left with as prepared CdS CQDs with

bright yellow color.
For the doped samples, the reaction mechanism remains the same with only addition of the following reaction at step 2.

$$Pb(CH_3COO)_2 \cdot 3H_2O(aq) \rightarrow Pb^{2+} + 2CH_3COO^- + 2H_2O$$

It can be understood that both Cd^{2+} and Pb^{2+} ions are present before the addition of the S^{2-} precursor, now the question is which cation while have the higher tendency to react first with the anion? This question can be answered by considering the electropositivity and reactivity of both species. Generally, cadmium has a higher tendency to lose electrons and form positive ions compared to lead, hence, Cd^{2+} is expected to readily form ionic bonds with S^{2-} due to its higher reactivity than Pb^{2+}.

Chapter 4

Results and Discussion

This section presents a comprehensive analysis of the experimental findings obtained from the synthesis and characterization of Pb-doped CdS colloidal quantum dots. This section includes the outcomes of the optical and electrical characterization studies mentioned in the previous section. The subsequent discussion delves into the interpretation and analysis of the results, focusing on the observed changes in absorption spectra, photoluminescence behavior, and electrical conductivity. The significance of these findings is explored, considering the implications for the Burstein-Moss effect and the potential applications of the doped quantum dots.

4.1 Experimental Synthesis Results

Following the procedure stated in chapter 3 for the preparation of the pure and doped colloidal samples, the as-prepared CQDs had a bright yellow, luminescent color typical of CdS compound. However, as the doping amount of Pb increased the samples showed a fading of this bright yellow color as seen in the figure below.

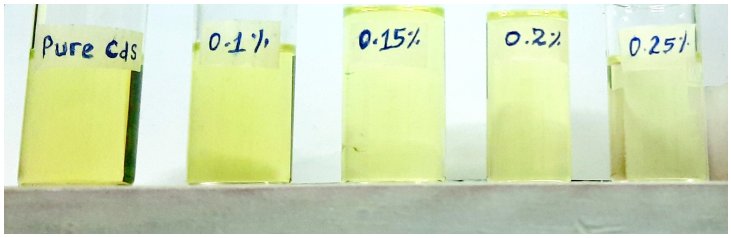

Figure 4.1: Pb-doped CdS Colloidal Quantum Dots

The synthesized Pb-doped CdS CQDs exhibited a vibrant bright yellow color. The incorporation of Pb dopant atoms into the CdS QDs resulted in a noticeable color shift compared to the undoped CdS QDs. The bright yellow hue indicates the successful formation of Pb-doped CdS QDs with a controlled dopant concentration. The color intensity and saturation may vary depending on the dopant concentration and the size of the QDs. The yellow coloration is attributed to the quantum confinement effect, where the size-dependent bandgap of the Pb-doped CdS QDs allows for the absorption and emission of light in the visible spectrum, particularly in the yellow region. This visually striking yellow coloration makes the

Pb-doped CdS CQDs highly desirable for various applications, including optoelectronics, display technologies, and colorimetric sensing.

4.2 Optical Characterization Results

UV-Vis Spectroscopy

The UV-Vis spectroscopy results of Pb-doped CdS CQDs exhibit an interesting behavior, showing a red shift followed by a subsequent blue shift upon increased dopant concentration as shown below.

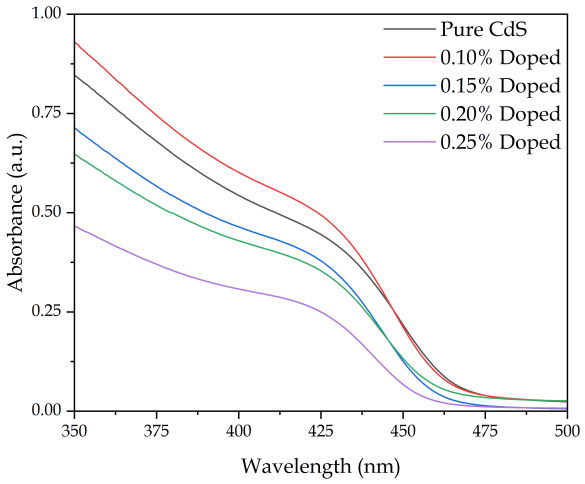

Figure 4.2: UV-Vis Spectroscopy Normalized Absorbance Plot for the studied samples

Initially, with a low dopant concentration, the absorption spectra of the Pb-doped CdS QDs demonstrate a red shift compared to undoped CdS QDs. This red shift indicates a decrease in the bandgap energy of the doped QDs. It suggests that the introduction of Pb dopant atoms into the CdS QDs modifies the electronic structure, resulting in a lowered bandgap and a shift towards longer wavelengths in the absorption spectra.

However, as the dopant concentration is further increased, a subsequent blue shift is observed in the absorption spectra of the Pb-doped CdS CQDs. This blue shift implies an increase in the bandgap energy, indicating the widening of the bandgap due to the higher dopant concentration. The blue shift is attributed to the Burstein-Moss effect, where the heavy doping leads to bandgap widening and a shift of the absorption edge towards shorter wavelengths or higher energies. Sivaraman *et al*[99], Rajashree *et al*[100] and Anbarasi *et al*[101], have reported similar results. They have mentioned that the red shift in optical bandgap

value was probably due to internal microstrain or stoichiometry while the blueshift under high doping is attributed to the Burstein-Moss effect, according to which the Pb^{2+} ions cause an increase in free carrier concentration which lifts the Fermi level into higher energy levels[99]–[101].

The presence of both the initial red shift and subsequent blue shift in the UV-Vis spectra of Pb-doped CdS CQDs is an intriguing result. It suggests a complex interplay between the dopant concentration, the electronic structure, and the resulting optical properties of the doped QDs. These findings have important implications for understanding the influence of dopant concentration on the optical behavior of the quantum dots and provide insights for tailoring their absorption properties for specific applications such as optoelectronics and photovoltaics.

Optical Bandgap Determination & Particle Size Estimation

The Tauc Plot (Fig. 4.3) which was obtained using Eq. 3.8, confirms an initial decrease in bandgap for 0.10% Pb-doped CdS CQDs then upon higher incorporation of dopant concentration a gradual increase in bandgap is observed.

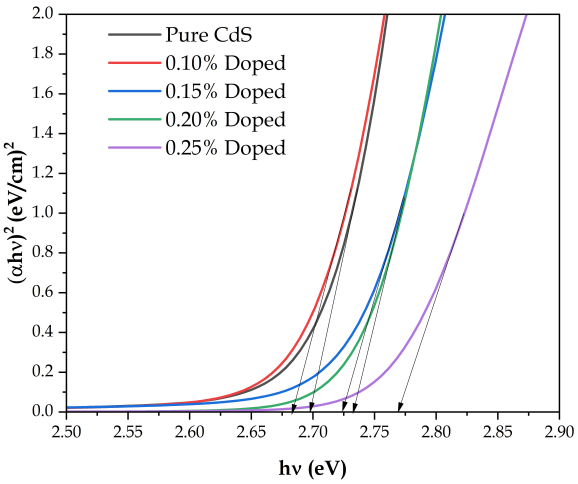

Figure 4.3: Tauc Plot for the studied samples

∗The optical bandgap values E_g were determined using the Tauc Plot using Eq. 3.8

∗∗ The nanoparticle size D was estimated using Eq. 3.10 where $D = 2R$

Starting from the pure sample having an optical bandgap of 2.70eV, we can observe an increase of bandgap from the bulk value of CdS (2.42eV), which shows that quantum confinement effect is at play. However, the introduction of dopant atoms affects the formation and

Table 4.1: Determination of Optical bandgap and particle size using optical studies

Sample	Absorbance Peak (nm)	Emission Peak (nm)	E_g^{QD} (eV)*	Estimated Size D (nm)**
Pure CdS	428	517	2.70	5.67
0.10% Doped	429	521	2.67	6.00
0.15% Doped	423	514	2.72	5.48
0.20% Doped	422	510	2.74	5.30
0.25% Doped	419	439	2.77	5.07

growth of the QDs. The presence of dopants can modify the nucleation and growth kinetics, leading to an increase in particle size. This initial increase in particle size can be explained by the reduced quantum confinement effect. The 0.10% doped sample has an estimated particle size of $D = 6nm$, which is greater than the exciton Bohr radius of CdS nanocrystals with $a_B = 5.8nm$[102]. This shows weak confinement as compared to the rest of the samples since $D > a_B$. For this reason, the confinement effect is less pronounced. As a result, the QDs can grow larger in size before the quantum confinement effect becomes significant.
As the dopant concentration is further increased, the quantum confinement effect becomes more prominent. The dopant atoms exert an influence on the nucleation and growth process, facilitating more efficient formation of smaller-sized QDs. Additionally, it can be seen that D is less than the Bohr radius for CdS nanocrystals, which shows that the nanocrystals are entering the strong confinement region. Consequently, the confinement effect restricts the spatial extent of the charge carriers within the QDs, thus confining them to smaller dimensions and resulting in a decrease in particle size. Further increment of Pb doping to 0.30% resulted in the loss of colloidal stability of the CdS CQDs, elucidating that the host CdS crystal lattice can not further accommodate the extra Pb atoms resulting in precipitation. This tells us that at 0.25% Pb concentration, the CdS is degenerately doped, further increased doping results in precipitation as proven experimentally.

Photoluminescence

The PL study of the Pb-doped CdS CQDs excited at $\lambda_{exc} = 280nm$ revealed a fascinating trend similar to the UV-Vis study: an initial redshift in the emitted light upon doping, followed by a noticeable blueshift at higher doping concentrations.
At low doping concentrations of Pb (0.10%) in the CdS CQDs, the introduction of Pb impurities caused the emission wavelength to undergo a redshift. This red shift indicated a longer wavelength emission compared to the undoped CdS CQDs. The incorporation of Pb impurities into the CdS lattice modified the band structure and energy levels of the QDs, leading

to a shift towards longer wavelengths in the emitted light. The redshift can be attributed to the changes in the confinement potential and bandgap due to the presence of the Pb impurities. However, as the doping concentration of Pb increased beyond a certain threshold, a significant change occurred. The increased doping resulted in the blue shift of the near band emissions, indicating a shorter wavelength emission compared to the initially doped sample. This blue shift suggested a higher energy emission. The change in emission behavior at higher doping concentrations can be attributed to various factors, such as the formation of Pb-rich clusters, the creation of defect states or BM shift due to excessive doping. These factors can influence the electronic structure and energy levels of the QDs, leading to a shift towards shorter wavelengths in the emitted light.

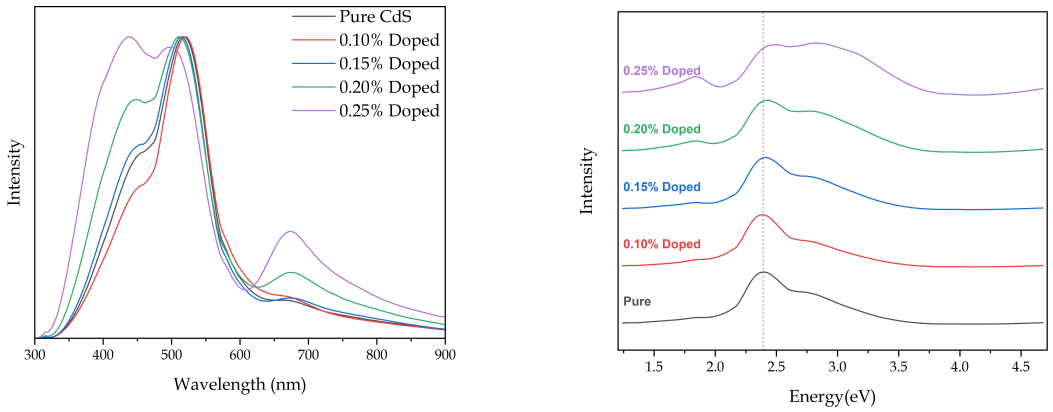

(a) **(b)**

Figure 4.4: (a) Photoluminescence Intensity vs. Wavelength Plot **(b)**Blue shiftting the Colloidal QDs upon increased doping

Additionally, one possible explanation for the blue shift is the band filling effect[103]. When additional Pb atoms are injected or introduced into the CdS CQDs, the carrier concentration increases, resulting in the available energy states in the conduction or valence band become more occupied, approaching a complete filling of the conduction band. This increased occupancy causes the Fermi level to lie inside the conduction band similar to the BM effect resulting in increased bandgap. Another outcome of doping we can observe is the increasing shoulder peaks of the near band emissions at higher energies and the deep level emissions at lower energies. While the former peaks represent doping induced vibronic transitions, the latter are more likely due to surface defects caused by increased doping.

Refractive Index, Dielectric Constant and Linear Optical Susceptibility

The table below summarizes the value of refractive index n, dielectric constant ϵ_r and linear optical susceptibility χ for the studied samples using the four empirical relations discussed in the previous chapter.

Table 4.2: Empirical Relations for Refractive Index, Dielectric Constant and Linear Optical Susceptibility

Sample	E_g (eV)	Herve & Vandamme Relation			Tripathy Relation			Ravindra Relation			Moss Relation		
		n	ϵ_r	χ	n	ϵ_r	χ	n	ϵ_r	χ	n	ϵ_r	χ
Pure CdS	2.70	2.444	5.973	4.973	2.498	6.240	5.240	2.410	5.808	4.808	2.440	5.954	4.954
0.10% Doped	2.67	2.454	6.022	5.022	2.510	6.30	5.30	2.430	5.905	4.905	2.442	5.963	4.963
0.15% Doped	2.72	2.440	5.954	4.954	2.489	6.20	5.20	2.40	5.760	4.760	2.431	5.910	4.910
0.20% Doped	2.74	2.430	5.905	4.905	2.481	6.160	5.160	2.390	5.712	4.712	2.430	5.905	4.905
0.25% Doped	2.77	2.420	5.860	4.860	2.470	6.101	5.101	2.370	5.617	4.617	2.420	5.856	4.856

The refractive index of a material describes how light propagates through it, specifically how much the speed and direction of light change when it enters the material. On the other hand, the bandgap represents the energy difference between the valence band (occupied electron states) and the conduction band (unoccupied electron states) in a material. In most cases, an increasing bandgap is associated with a decrease in the refractive index[97]. This relationship can be understood by considering the interaction of light with the electronic structure of a material. When light passes through a medium, it can interact with the electrons in that material, causing absorption and subsequent re-emission. In materials with a smaller bandgap, the energy levels available for electronic transitions are closer together. As a result, light with a wider range of energies (wavelengths) can be absorbed and re-emitted by the material. This absorption and re-emission process affects the speed of light passing through the material, resulting in a higher refractive index.

On the other hand, materials with a larger bandgap have a larger energy difference between the valence and conduction bands. In such materials, only higher energy photons (corresponding to shorter wavelengths) can be absorbed and promote electrons to the conduction band. As a result, there is less interaction between light and the electrons in the material, leading to lower absorption and a lower refractive index.

The comparison shows that the data obtained for the Pb-doped CdS CQDs agree well the theoretical foundation where the optical parameters n, ϵ_r and χ decrease as E_g increases. Furthermore, the Herve and Vandamme and Moss relation are observed to coincide with eachother having similar values.

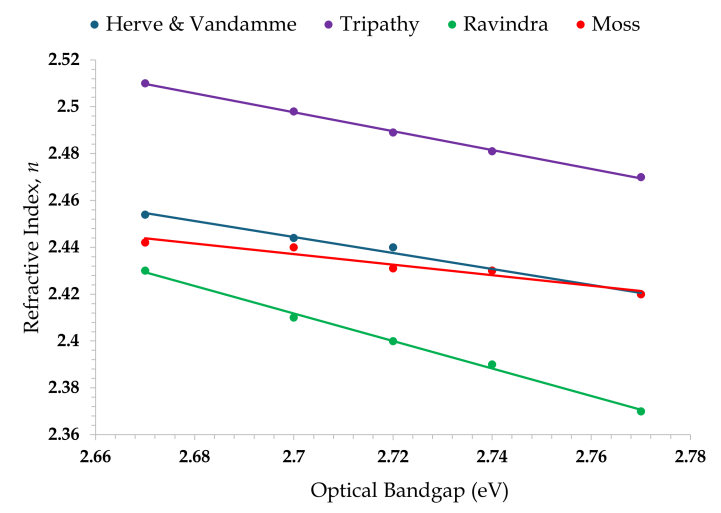

Figure 4.5: Comparison between Empirical Relations for Refractive Index and E_g

Fourier Transform Infrared Spectroscopy

The properties of the doped colloidal quantum dots were studied under infrared light to look into their chemical composition and bonds. The FTIR plot for the pure sample (Fig. 4.6) has similar peaks to the ones obtained by Órdenes-Aenishanslins *et al*[104]. Albeit the peak values show variation due to the introduction of the dopant and the chemical synthesis method used.

The infrared characterization interaction among the QDs revealed various peaks. In each spectrum or sample, the broad peaks at $3305cm^{-1}$ in the functional group region are attributed to the effect of hydroxyl (-OH) group stretching vibration[105]. Additionally, the node at $2150cm^{-1}$ can be attributed to the thiocynate ($S-C\equiv N$) stretching which originates from the sulfur precursor i.e. thiourea. The $1631cm^{-1}$ medium peak is caused by either C=C stretching or N-H bending. The $1403cm^{-1}$ small peak is a result of alkane (C-H) bending contained in the acetate group. These functional groups arise from the various precursor sources used during synthesis.

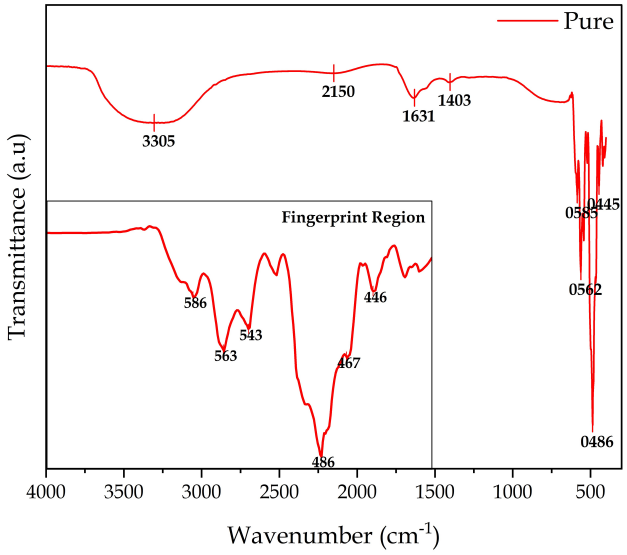

Figure 4.6: FTIR for Pure CdS Colloidal QDs with Fingerprint Region Inset

Interestingly, the fingerprint region contains peaks less than $600cm^{-1}$ which are commonly attributed to the Cd-S stretching mode[106].

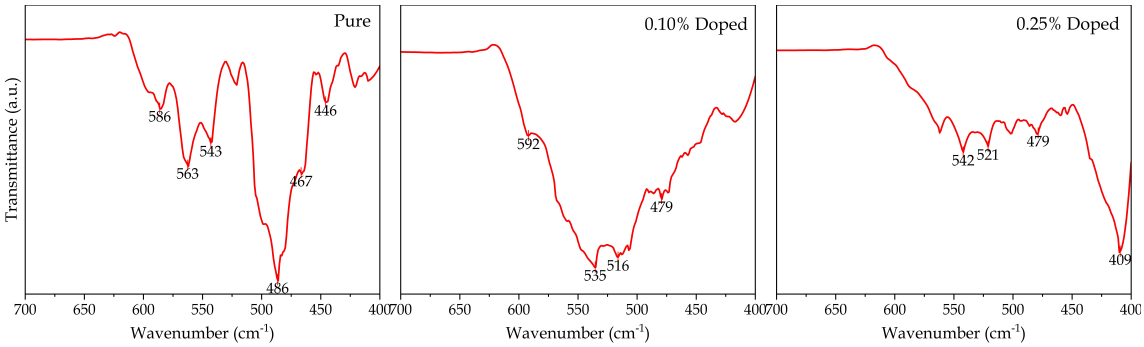

Figure 4.7: Fingerprint Region of the FTIR Spectra for Pure, 0.10% and 0.25% Doped Samples

However, an appreciable change in peak values of this region was observed upon Pb doping (Fig. 4.7). The introduction of Pb atoms into the CdS CQDs has changed the outcome of the FTIR spectra showing that there was a change in molecular vibrations or stretching. One reason may be due to stress and strain effects. Degenerate doping can introduce stress or strain within the crystal lattice of the material. This stress/strain can affect the molecular vibrations causing strain-induced modifications in the molecular structure. Additionally, due to the seemingly increased carrier concentration attributed to the Burstein-Moss effect, there

is a possibility that the local electric field is affected which then alters the polarizability of the doped CdS CQDs. These carrier-induced effects can manifest as shifts or intensity changes in the FTIR peaks, particularly in the fingerprint region. Lastly, degenerate doping may introduce dopant related defects within the QDs. These defects act as additional vibrational centers, leading to shifts or appearance of new peaks.

4.3 Electrical Characterization Results

It is known that native defects such as S vacancies or Cd interstitials contribute to electrical conductivity of pure CdS. Hence, by controlling those native defects it is possible to enhance the electrical properties.

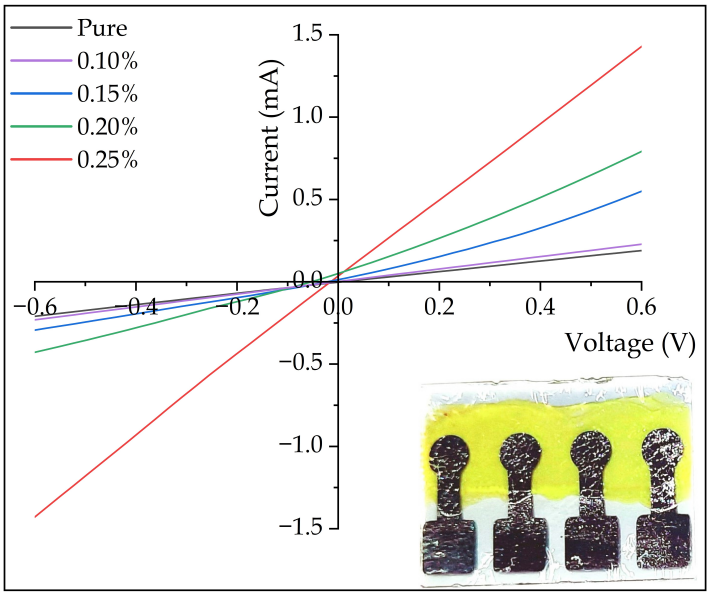

Figure 4.8: I-V Curve Comparison of Electrical Properties of the Synthesized Samples

The electrical resistivity measurements summarized in table 4.3 showed that CdS:Pb samples have resistivity in the order of $10^4 \Omega cm$. The order of resistivity obtained here exactly matches with the values reported by Sivaraman *et al*[99]. For undoped CdS CQDs ,the resistivity is found to be $0.3064 \times 10^4 \Omega cm$. For the CdS:Pb samples, the calculated resistivity values were found to be equal to $0.2616 \times 10^4 \Omega cm$, $0.1569 \times 10^4 \Omega cm$, $0.1036 \times 10^4 \Omega cm$, $0.0431 \times 10^4 \Omega cm$ for the CQDs with 0.10%, 0.15%, 0.20% and 0.25% at Pb concentrations respectively. The reduction in the resistivity of CdS:Pb samples is due to increased carrier concentration attributed to substitutional incorporation of Pb ions in the CdS structure. Also the reduction of the resistivity can be attributed to the rise of carriers due to sulfur deficiencies.

Table 4.3: Electrical Properties of the synthesised Samples

Samples	**Conductance (G)** $(10^{-4}\Omega^{-1})$	**Resistance (R)** $(10^{4}\Omega)$	**Conductivity** σ $(10^{-4}[\Omega cm]^{-1})$
Pure CdS	3.264	0.3064	3.264
0.10% Doped	3.822	0.2616	3.822
0.15% Doped	6.372	0.1569	6.372
0.20% Doped	9.656	0.1036	9.656
0.25% Doped	23.2	0.0431	23.2

One possible explanation is that as the doping concentration increases, annihilation of Cd vacancies (acceptor centers) and S Vacancies (donors) takes place with a beneficial situation being created for the incorporation of Pb atoms on the unoccupied S vacancy sites, there by increasing the electron concentration which results in the decrease in the resistivity of the doped CQDs, with increased content of Pb. Figure 4.8 shows that the electrical conductivity behaviour of the colloidal samples is ohmic or linear. While the conductivity of the 0.25% Pb doped sample is greatly improved by around 7 times from the pure CdS CQDs sample, further optimization of its conductivity and optical properties is required to use it for photovoltaic purposes such as in active layer or as a window/buffer layer.

Chapter 5

Conclusion

In this work, the doping effect of Pb atoms was investigated on the optoelectronic properties of CdS CQDs. Firstly, the concept of quantum confinement was explored through the theories of Quantum Mechanics. The confinement energy from the effective mass approximation was derived using the time-independent Schrödinger Equation. This approximation method unveiled that the bandgap of the QDs was dependent on E_g^{Bulk}, E_{Conf}, E_{exc} and E_{Ryd}. Following the experimental route, CdS CQDs were synthesized using a modified version of chemical bath deposition technique. The resulting CQDs had a bright yellow vibrant color. The UV-Vis and PL studies both showed an initial redshift followed by blueshift at increased Pb concentrations. Using Tauc Plot, the bandgap values were found to be 2.70eV, 2.67eV, 2.72eV, 2.74eV and 2.77eV for pure, 0.10%, 0.15%, 0.20% and 0.25% doped samples respectively. The increase in bandgap at higher concentration was attributed to the Burstein-Moss shift. The FTIR characterization showed the effect of Pb doping through having shifts and intensity changes in peak values of the fingerprint region, showing that the Pb caused variation in molecular vibrations and stretching. Further analysis was done to determine the refractive index, dielectric constant and linear optical susceptibility from the optical bandgaps using empirical relations. It was found that all three optical parameters decreased upon increasing bandgap which is consistent with many literatures. Finally, electrical characterization was done to determine the resistivity and conductivity of the samples in thin film form. It was noted that upon increased Pb concentration, the resistivity decreased resulting in augmented conductivity by upto 7 times from the undoped sample. Additionally, the IV curve of the studied samples had ohmic nature showing the samples resemble a metallic conductor.

Future Work

While Pb-doped CdS CQDs were successfully synthesized and studied, further optimization is required to ensure the colloidal stability of the CQDs. It was observed that the prepared samples in this study had stability lasting 5-7 days before noticeable precipitation was observed. Moreover, the colloidal samples had weak adhesion to glass substrate resulting in uneven formation of thin films. For use in hybrid photovoltaic devices as an active layer or buffer/window layer, the polarity of the CdS CQDs must be investigated. Due to the ionic

interaction in the CdS, the resulting solution is strongly polar and insoluble in organic solvents like chloroform or ODCB. Hence, ligand exchange methods can be looked into for the successful formation of bulk heterojunction layer with for example, known polymer poly(3-hexylthiophene-2,5-diyl) (P3HT). Furthermore, since the parabolic band approximation model was inadequate to fully describe the properties of the CQDs, new models especially computational approach to determine the carrier concentration value n should be topic of future research.

References

[1] W. J. Parak, L. Manna, F. C. Simmel, D. Gerion, and P. Alivisatos, "Quantum dots," in *Nanoparticles*. John Wiley & Sons, Ltd, 2010, ch. 2, pp. 3–47, ISBN: 9783527631544.

[2] K. Gajanan and S. N. Tijare, "Applications of nanomaterials," *Materials Today: Proceedings*, vol. 5, pp. 1093–1096, Jan. 2018.

[3] R. Feynman, "There's plenty of room at the bottom," 1959.

[4] M. A. Cotta, "Quantum dots and their applications: What lies ahead?" *ACS Appl. Nano Mater.*, vol. 3, no. 6, pp. 4920–4924, Jun. 2020.

[5] L. Schiavo, A. Cammarano, G. Carotenuto, A. Longo, M. Palomba, and L. Nicolais, "An overview of the advanced nanomaterials science," *Inorganica Chimica Acta*, vol. 559, Jan. 2024.

[6] T. R. S. A. of Sciences, "The discovery and development of quantum dots," *Nobel Prize*, 2023.

[7] S. Gangasani and B. Student, "A study on quantum dot and its applications," *International Journal of Innovative Research in Science, Engineering and Technology*, vol. 5, no. 5, pp. 8128–8133, 2016.

[8] D. Bera, L. Qian, T.-K. Tseng, and P. H. Holloway, "Quantum dots and their multimodal applications: A review," en, *Materials (Basel)*, vol. 3, no. 4, pp. 2260–2345, Mar. 2010.

[9] A. P. Alivisatos, "Semiconductor clusters, nanocrystals, and quantum dots," *Science*, vol. 271, no. 5251, pp. 933–937, 1996.

[10] N. Soltani, E. Saion, M. Z. Hussein, *et al.*, "Visible light-induced degradation of methylene blue in the presence of photocatalytic ZnS and CdS nanoparticles," *International Journal of Molecular Sciences*, vol. 13, no. 10, pp. 12 242–12 258, 2012.

[11] M. Di Ventra, S. Evoy, and J. Heflin, *Introduction to Nanoscale Science and Technology*. Jan. 2004, p. 184.

[12] P. Yu and M. Cardona, "Fundamentals of semiconductors," *Fundamentals of Semiconductors. Graduate Texts in Physics. Edited by Cardona, Manuel. Berlin: Springer, 2010.*, Jan. 2010.

[13] R. Gopal, P. Kathirgamanathan, G. Ravi, *et al.*, "Quantum confinement effect of 2D nanomaterials," in IntechOpen, Aug. 2020.

[14] S. M. Sze and K. K. Ng, *Physics of Semiconductor Devices*, 3rd. John Wiley & Sons, Ltd, 2007.

[15] N. Prodanović, "Semiconductor quantum dots: Intraband electronic, optical and carrier dynamical properties," Ph.D. dissertation, Apr. 2014.

[16] S. Hoogland, "The Fuss about quantum dots," *Photonics Spectra*, 2024.

[17] L. E. Brus, "Electron–electron and electron-hole interactions in small semiconductor crystallites: The size dependence of the lowest excited electronic state," *The Journal of Chemical Physics*, vol. 80, no. 9, pp. 4403–4409, May 1984.

[18] C. Delerue and M. Lannoo, "Quantum confined systems," in *Nanostructures: Theory and Modeling*. Springer Berlin Heidelberg, 2004, pp. 47–76.

[19] C. Delerue and M. Lannoo, *Nanostructures: Theory and Modelling* (NanoScience and Technology). Springer, 2004.

[20] C. Vatankhah and A. Ebadi, "Quantum size effects on effective mass and band gap of semiconductor quantum dots," *Res. J. Recent Sci.*, vol. 2, pp. 21–24, Jan. 2013.

[21] Y.-S. Huang, K.-T. Wu, and C.-H. Wu, "The right way to solve the infinite spherical well in quantum mechanics," Jul. 2017.

[22] Y. Kayanuma, "Quantum-size effects of interacting electrons and holes in semiconductor microcrystals with spherical shape," *Phys. Rev. B*, vol. 38, pp. 9797–9805, 14 Nov. 1988.

[23] F. Hone, F. Ampong, T. Abza, I. Nkrumah, R. Nkum, and F. Boakye, "Synthesis and characterization of CdSe nanocrystalline thin film by chemical bath deposition technique," *Int. J. Thin. Fil. Sci. Tec*, vol. 4, pp. 69–74, Jan. 2015.

[24] J. M. Pietryga, Y.-S. Park, J. Lim, *et al.*, "Spectroscopic and device aspects of nanocrystal quantum dots," *Chemical Reviews*, vol. 116, no. 18, pp. 10 513–10 622, 2016.

[25] M. Liu, O. Voznyy, R. Sabatini, *et al.*, "Hybrid organic–inorganic inks flatten the energy landscape in colloidal quantum dot solids," *Nature Materials*, vol. 16, no. 2, pp. 258–263, Feb. 2017.

[26] M. R. Kim and D. Ma, "Quantum-dot-based solar cells: Recent advances, strategies, and challenges," *The Journal of Physical Chemistry Letters*, vol. 6, no. 1, pp. 85–99, 2015.

[27] F. P. García de Arquer, A. Armin, P. Meredith, and E. H. Sargent, "Solution-processed semiconductors for next-generation photodetectors," *Nature Reviews Materials*, vol. 2, no. 3, p. 16 100, Jan. 2017.

[28] Y. E. Panfil, M. Oded, and U. Banin, "Colloidal quantum nanostructures: Emerging materials for display applications," *Angewandte Chemie International Edition*, vol. 57, no. 16, pp. 4274–4295, 2018.

[29] C. R. Kagan, E. Lifshitz, E. H. Sargent, and D. V. Talapin, "Building devices from colloidal quantum dots," *Science*, vol. 353, no. 6302, aac5523, 2016.

[30] B. Pelaz, C. Alexiou, R. A. Alvarez-Puebla, *et al.*, "Diverse applications of nanomedicine," *ACS Nano*, vol. 11, no. 3, pp. 2313–2381, 2017.

[31] G. Xu, S. Zeng, B. Zhang, M. T. Swihart, K.-T. Yong, and P. N. Prasad, "New generation cadmium-free quantum dots for biophotonics and nanomedicine," *Chemical Reviews*, vol. 116, no. 19, pp. 12 234–12 327, 2016.

[32] I. L. Medintz, H. T. Uyeda, E. R. Goldman, and H. Mattoussi, "Quantum dot bioconjugates for imaging, labelling and sensing," *Nature Materials*, vol. 4, no. 6, pp. 435–446, Jun. 2005.

[33] M. A. Cotta, "Quantum dots and their applications: What lies ahead?" *ACS Applied Nano Materials*, vol. 3, no. 6, pp. 4920–4924, 2020.

[34] Y. Shirasaki, G. J. Supran, M. G. Bawendi, and V. Bulović, "Emergence of colloidal quantum-dot light-emitting technologies," *Nature Photonics*, vol. 7, no. 1, pp. 13–23, Jan. 2013.

[35] S. Kubendhiran, Z. Bao, K. Dave, and R.-S. Liu, "Microfluidic synthesis of semiconducting colloidal quantum dots and their applications," *ACS Applied Nano Materials*, vol. 2, no. 4, pp. 1773–1790, 2019.

[36] G. Chen, J. Seo, C. Yang, and P. N. Prasad, "Nanochemistry and nanomaterials for photovoltaics," *Chem. Soc. Rev.*, vol. 42, pp. 8304–8338, 21 2013.

[37] R. K. Kokal, A. R. C. Bredar, B. H. Farnum, and M. Deepa, "Solid-state succinonitrile/sulfide hole transport layer and carbon fabric counter electrode for a quantum dot solar cell," *ACS Applied Nano Materials*, vol. 2, no. 12, pp. 7880–7887, 2019.

[38] S. Gudjonsdottir, W. van der Stam, C. Koopman, B. Kwakkenbos, W. H. Evers, and A. J. Houtepen, "On the stability of permanent electrochemical doping of quantum dot, fullerene, and conductive polymer films in frozen electrolytes for use in semiconductor devices," *ACS Applied Nano Materials*, vol. 2, no. 8, pp. 4900–4909, 2019.

[39] D. Bederak, D. M. Balazs, N. V. Sukharevska, *et al.*, "Comparing halide ligands in pbs colloidal quantum dots for field-effect transistors and solar cells," *ACS Applied Nano Materials*, vol. 1, no. 12, pp. 6882–6889, 2018.

[40] R. Bose, A. Dangerfield, S. M. Rupich, *et al.*, "Engineering multilayered nanocrystal solids with enhanced optical properties using metal oxides for photonic applications," *ACS Applied Nano Materials*, vol. 1, no. 12, pp. 6782–6789, 2018.

[41] L. Liu, S. Z. Bisri, Y. Ishida, D. Hashizume, T. Aida, and Y. Iwasa, "Ligand and solvent effects on hole transport in colloidal quantum dot assemblies for electronic devices," *ACS Applied Nano Materials*, vol. 1, no. 9, pp. 5217–5225, 2018.

[42] Q. Dong, H. Liu, Y. Hara, H. E. Starr, J. L. Dempsey, and R. Lopez, "Impact of background oxygen pressure on the pulsed-laser deposition of zno nanolayers and on their corresponding performance as electron acceptors in pbs quantum-dot solar cells," *ACS Applied Nano Materials*, vol. 2, no. 2, pp. 767–777, 2019.

[43] M. A. Mumin, K. F. Akhter, O. O. Oyeneye, W. Z. Xu, and P. A. Charpentier, "Supercritical fluid assisted dispersion of nano-silica encapsulated CdS/ZnS quantum dots in poly(ethylene-co-vinyl acetate) for solar harvesting films," *ACS Applied Nano Materials*, vol. 1, no. 7, pp. 3186–3195, 2018.

[44] T. Sivaraman, A. Balu, and V. Nagarethinam, "Effect of magnesium incorporation on the structural, morphological, optical and electrical properties of CdS thin films," *Materials science in semiconductor processing*, vol. 27, pp. 915–923, 2014.

[45] M. Anbarasi, V. Nagarethinam, and A. Balu, "Investigations on the structural, morphological, optical and electrical properties of undoped and nanosized Zn-doped CdS thin films prepared by a simplified spray technique," *Materials Science-Poland*, vol. 32, pp. 652–660, 2014.

[46] N. Shah, R. Sagar, W. Mahmood, and W. Syed, "Cu-doping effects on the physical properties of cadmium sulfide thin films," *Journal of Alloys and Compounds*, vol. 512, no. 1, pp. 185–189, 2012.

[47] N. Badera, B. Godbole, S. Srivastava, *et al.*, "Quenching of photoconductivity in Fe doped CdS thin films prepared by spray pyrolysis technique," *Applied surface science*, vol. 254, no. 21, pp. 7042–7048, 2008.

[48] S. Mane, P. Pingale, R. Suryawanshi, V. Karande, L. Deshmukh, and M. Sharon, "On the surface morphology and transport properties of chemical bath deposited $Co_xCd_{1-x}S$ thin films: A correlation," *Electrochimica Acta*, vol. 114, pp. 494–499, 2013.

[49] J. D. Rinehart, A. M. Schimpf, A. L. Weaver, A. W. Cohn, and D. R. Gamelin, "Photochemical electronic doping of colloidal CdSe nanocrystals," *J. Am. Chem. Soc.*, vol. 135, no. 50, pp. 18 782–18 785, Dec. 2013.

[50] L. Hu, Q. Lei, X. Guan, *et al.*, "Optimizing surface chemistry of PbS colloidal quantum dot for highly efficient and stable solar cells via chemical binding," *Advanced Science*, vol. 8, no. 2, p. 2 003 138, 2021.

[51] L. Yu, P. Tian, L. Tang, *et al.*, "Room temperature broadband Bi_2Te_3/PbS colloidal quantum dots infrared photodetectors," *Sensors*, vol. 23, no. 9, p. 4328, 2023.

[52] L. Meng and X. Wang, "Doping colloidal quantum dot materials and devices for photovoltaics," *Energies*, vol. 15, no. 7, p. 2458, 2022.

[53] C. Yadav and B. Bhattacharya, "Synthesis of CdS quantum dots at various temperatures," Ph.D. dissertation, May 2018.

[54] S. Prasad, M. Raja, and M. Joseph, "Synthesis of CdS quantum dots by reverse micelle method," pp. 38–39, Jul. 2013.

[55] X. Zheng, J. Weng, and B. Hu, "Microwave-assisted synthesis of mesoporous CdS quantum dots modified by oleic acid," *Materials science in semiconductor processing*, vol. 13, no. 3, pp. 217–220, 2010.

[56] T. Abza and F. G. Hone, "Synthesizing lanthanum doped cadmium sulfide thin films for photovoltaic application," 2019.

[57] S. Reda, "Synthesis and optical properties of CdS quantum dots embedded in silica matrix thin films and their applications as luminescent solar concentrators," *Acta Materialia*, vol. 56, no. 2, pp. 259–264, 2008.

[58] P. Jadhav, G. Bhand, K. Mohite, and N. Chaure, "CdS quantum dots synthesized by low-cost wet chemical technique," *AIP Conference Proceedings*, vol. 1832, p. 050 146, May 2017.

[59] Y. Chen and Z. Rosenzweig, "Luminescent CdS quantum dots as selective ion probes," *Anal. Chem.*, vol. 74, no. 19, pp. 5132–5138, Oct. 2002.

[60] W.-T. Sun, Y. Yu, H.-Y. Pan, X.-F. Gao, Q. Chen, and L.-M. Peng, "CdS quantum dots sensitized TiO2 Nanotube-Array photoelectrodes," *J. Am. Chem. Soc.*, vol. 130, no. 4, pp. 1124–1125, Jan. 2008.

[61] G.-S. Li, D.-Q. Zhang, and J. C. Yu, "A new visible-light photocatalyst: CdS quantum dots embedded mesoporous tio2," *Environmental science & technology*, vol. 43, no. 18, pp. 7079–7085, 2009.

[62] H. Li, W. Y. Shih, and W.-H. Shih, "Synthesis and characterization of aqueous carboxyl-capped CdS quantum dots for bioapplications," *Industrial & engineering chemistry research*, vol. 46, no. 7, pp. 2013–2019, 2007.

[63] Y.-J. Shen and Y.-L. Lee, "Assembly of CdS quantum dots onto mesoscopic TiO2 films for quantum dot-sensitized solar cell applications," *Nanotechnology*, vol. 19, no. 4, p. 045 602, 2008.

[64] I. Devadoss, P. Sakthivel, and A. Krishnamoorthy, "Band gap tailoring and photoluminescence performance of CdS quantum dots for white led applications: Influence of Ba^{2+} and Zn^{2+} ions," *Journal of Materials Science: Materials in Electronics*, vol. 32, pp. 5729–5737, 2021.

[65] B. Poornaprakash, U. Chalapathi, P. Poojitha, S. Prabhakar Vattikuti, and S.-H. Park, "Influence of gadolinium (iii) doping on the structural, optical, magnetic, and photocatalytic properties of CdS quantum dots," *Materials Science in Semiconductor Processing*, vol. 100, pp. 73–78, 2019, ISSN: 1369-8001.

[66] A. Ganguly and S. Nath, "Mn-doped CdS quantum dots as sensitizers in solar cells," *Materials Science and Engineering: B*, vol. 255, p. 114 532, 2020, ISSN: 0921-5107.

[67] M. Shkir, M. Anis, S. Shafik, *et al.*, "An effect of zn content doping on opto-third order nonlinear characteristics of nanostructured CdS thin films fabricated through spray pyrolysis for optoelectronics," *Physica E: Low-dimensional Systems and Nanostructures*, vol. 118, p. 113 955, 2020, ISSN: 1386-9477.

[68] M. Muthusamy and S. Muthukumaran, "Effect of cu-doping on structural, optical and photoluminescence properties of CdS thin films," *Optik*, vol. 126, no. 24, pp. 5200–5206, 2015, ISSN: 0030-4026.

[69] M. Thambidurai, N. Muthukumarasamy, S. Agilan, N. Sabari Arul, N. Murugan, and R. Balasundaraprabhu, "Structural and optical characterization of ni-doped CdS quantum dots," *Journal of Materials Science*, vol. 46, no. 9, pp. 3200–3206, May 2011.

[70] Z. K. Heiba, M. B. Mohamed, and N. Y. Mostafa, "Effect of V and Y doping on the structural, optical and electronic properties of CdS (hexagonal and cubic phases)," *Applied Physics A*, vol. 125, no. 2, p. 132, Jan. 2019.

[71] M. Thambidurai, N. Muthukumarasamy, S. Agilan, *et al.*, "Studies on optical absorption and structural properties of fe doped CdS quantum dots," *Solid State Sciences*, vol. 12, no. 9, pp. 1554–1559, Sep. 2010.

[72] P. Maity, S. Kumar, R. Kumar, *et al.*, "Role of cobalt doping in CdS quantum dots for potential application in thin film optoelectronic devices," *J. Phys. Chem. C*, vol. 125, no. 3, pp. 2074–2088, Jan. 2021.

[73] A. Firdous, D. Singh, and M. M. Ahmad, "Electrical and optical studies of pure and ni-doped CdS quantum dots," *Applied Nanoscience*, vol. 3, no. 1, pp. 13–18, Feb. 2013.

[74] P. M. Tan, N. X. Ca, N. T. Hien, *et al.*, "New insights on the energy transfer mechanisms of eu-doped CdS quantum dots," *Phys. Chem. Chem. Phys.*, vol. 22, no. 11, pp. 6266–6274, 2020.

[75] B. Mullamuri, V. Sai, V. S. S. Mosali, H. Maseed, S. Majety, and B. Chandu, "Photocatalytic activity of heavy metal doped CdS nanoparticles synthesized by using ocimum sanctum leaf extract," *Biointerface Research in Applied Chemistry*, vol. 11, pp. 12 547–12 559, Jan. 2021.

[76] K. Veerathangam, M. S. Pandian, and P. Ramasamy, "Photovoltaic performance of pb-doped CdS quantum dots for solar cell application," *Materials Letters*, vol. 220, pp. 74–77, 2018.

[77] C. Yuan, L. Li, J. Huang, Z. Ning, L. Sun, and H. Ågren, "Improving the photocurrent in Quantum-Dot-Sensitized solar cells by employing alloy Pb(x)Cd(1-x)S quantum dots as photosensitizers," *Nanomaterials*, vol. 6, no. 6, 2016.

[78] M. Guglielmi, A. Martucci, J. Fick, and G. Vitrant, "Preparation and characterization of Hg(x)Cd(1-x)S and Pb(x)Cd(1-x)S quantum dots and doped thin films," *Journal of sol-gel science and technology*, vol. 11, pp. 229–240, 1998.

[79] G. H. Fekadu, "Synthesis and characterization of cadmium selenide CdSe and lead sulphur selenide $PbS_{1-x}Se_x$ thin films by chemical bath deposition method," Ph.D. dissertation, 2015.

[80] A. I. Oliva, I. J. González-Chan, P. E. Várguez, A. I. Trejo-Ramos, and A. I. Oliva-Avilés, "The chemical process for materials deposition in aqueous solution: A review," *Surface Engineering*, vol. 38, no. 10-12, pp. 907–929, 2022.

[81] M. R. D. Guire, L. P. Bauermann, H. Parikh, and J. Bill, "Chemical bath deposition," *Chemical solution deposition of functional oxide thin films*, pp. 319–339, 2013.

[82] F. G. Hone and F. B. Dejene, "Chemosynthesis of nanostructures lead sulphide thin films from triethylamin (et3n) complexing agent," *Inorganic Chemistry Communications*, vol. 111, p. 107 583, 2020.

[83] F. T. Geldasa, M. A. Kebede, S. Z. Werta, and F. G. Hone, "Chemical bath deposition approach to produce three different morphologies of PbO thin films from different cation concentrations," *Indian Journal of Physics*, pp. 1–11, 2024.

[84] D. Wang, T. He, S. Li, Y. Jiang, and M. Yuan, "Li-doped chemical bath deposited SnO_2 enables efficient perovskite photovoltaics," *ACS Applied Energy Materials*, vol. 5, no. 5, pp. 5340–5347, 2021.

[85] F. G. Hone, N. A. Tegegne, F. B. Dejene, and D. M. Andoshe, "Nanofiber cadmium oxide thin films prepared from ethanolamine complexing agent by solution growth method," *Optik*, vol. 243, p. 167 402, 2021.

[86] S. Shinde, H. Yadav, G. Ghodake, *et al.*, "Using chemical bath deposition to create nanosheet-like CuO electrodes for supercapacitor applications," *Colloids and Surfaces B: Biointerfaces*, vol. 181, pp. 1004–1011, 2019.

[87] X. Zou, H. Fan, Y. Tian, M. Zhang, and X. Yan, "Chemical bath deposition of Cu_2O quantum dots onto ZnO nanorod arrays for application in photovoltaic devices," *RSC Advances*, vol. 5, no. 30, pp. 23 401–23 409, 2015.

[88] K. L. Chopra, S. R. Das, K. L. Chopra, and S. R. Das, *Why thin film solar cells?* Springer, 1983.

[89] F. G. Hone, F. K. Ampong, T. Abza, I. Nkrumah, R. K. Nkum, and F. Boakye, "Investigating the effect of deposition time on the morphology, structure and optical band gap of pbs thin films synthesized by cbd technique," *Elixir Thin Film Tech*, vol. 76, pp. 28 432–28 437, 2014.

[90] D. G. Seiler, A. C. Diebold, R. McDonald, *et al.*, "Frontiers of characterization and metrology for nanoelectronics," 2009.

[91] J. Poppe, "Spectroelectrochemical investigations of semiconductor nanoparticles," 2015.

[92] O. Faix, "Fourier transform infrared spectroscopy," in *Methods in Lignin Chemistry*, S. Y. Lin and C. W. Dence, Eds. Berlin, Heidelberg: Springer Berlin Heidelberg, 1992, pp. 83–109.

[93] F. G. Hone and F. B. Dejene, "Synthesis lead sulphide thin films from tartaric acid chemical bath: Study the role of film thickness on the structural, optical and electrical properties," *Thin Solid Films*, vol. 692, 2019, ISSN: 0040-6090.

[94] P. Hervé and L. K. J. Vandamme, "General relation between refractive index and energy gap in semiconductors," *Infrared Physics & Technology*, vol. 35, no. 4, pp. 609–615, Jun. 1994.

[95] N. M. Ravindra, P. Ganapathy, and J. Choi, "Energy gap–refractive index relations in semiconductors – an overview," *Infrared Physics & Technology*, vol. 50, no. 1, pp. 21–29, Mar. 2007.

[96] S. K. Tripathy and A. Pattanaik, "Optical and electronic properties of some semiconductors from energy gaps," *Optical Materials*, vol. 53, pp. 123–133, Mar. 2016.

[97] S. K. Tripathy, "Refractive indices of semiconductors from energy gaps," *Optical Materials*, vol. 46, pp. 240–246, Aug. 2015.

[98] K. Saw, N. Aznan, F. Yam, S. S. Ng, and S. Pung, "New insights on the burstein-moss shift and band gap narrowing in indium-doped zinc oxide thin films," *PLOS ONE*, vol. 10, e0141180, Oct. 2015.

[99] T. Sivaraman, V. Narasimman, V. S. Nagarethinam, and A. R. Balu, "Effect of chlorine doping on the structural, morphological, optical and electrical properties of spray deposited CdS thin films," *Progress in Natural Science: Materials International*, vol. 25, no. 5, pp. 392–398, Oct. 2015.

[100] C. Rajashree, A. Balu, and V. Nagarethinam, "Properties of Cd doped PbS thin films: Doping concentration effect," *Surface Engineering*, vol. 31, pp. 316–321, Apr. 2015.

[101] M. Anbarasi, V. S. Nagarethinam, R. Baskaran, and V. Narasimman, "Studies on the structural, morphological and optoelectrical properties of spray deposited CdS:Pb thin films," *Pacific Science Review A: Natural Science and Engineering*, vol. 18, no. 1, pp. 72–77, Jan. 2016.

[102] R. S. Yadav, P. Mishra, R. Mishra, M. Kumar, and A. C. Pandey, "Growth mechanism and optical property of CdS nanoparticles synthesized using amino-acid histidine as chelating agent under sonochemical process," *Ultrasonics Sonochemistry*, vol. 17, no. 1, pp. 116–122, Jan. 2010.

[103] P. V. Kamat, N. M. Dimitrijevic, and A. J. Nozik, "Dynamic burstein-moss shift in semiconductor colloids," *The Journal of Physical Chemistry*, vol. 93, no. 8, pp. 2873–2875, 1989.

[104] N. Órdenes-Aenishanslins, G. Anziani-Ostuni, C. Quezada, R. Espinoza, D. Bravo, and J. Pérez-Donoso, "Biological synthesis of CdS/CdSe core/shell nanoparticles and its application in quantum dot sensitized solar cells," *Frontiers in Microbiology*, vol. 10, p. 1587, Jul. 2019.

[105] M. S. Abd El-sadek, D.-H. Wasly, and H. El-Sheshtawy, "$CdS@Mn(OH)_2$ nanocomposites: Novel aqueous synthesis, structural and optical properties," *The European Physical Journal Plus*, vol. 133, Dec. 2018.

[106] P. Maity, S. Kumar, R. Kumar, *et al.*, "Role of cobalt doping in CdS quantum dots for potential application in thin film optoelectronic devices," *J. Phys. Chem. C*, vol. 125, no. 3, pp. 2074–2088, Jan. 2021.